Synthesis, characterization and computational study of complexes containing Pt···H hydrogen bonding interactions

Miguel Baya, Úrsula Belío, and Antonio Martín*

Instituto de Síntesis Química y Catálisis Homogénea (ISQCH). Departamento de Química Inorgánica. Universidad de Zaragoza – CSIC. 50009 Zaragoza, Spain.
E mail: tello@unizar.es

Dedicated to Prof. Antonio Laguna on the occasion of his 65th birthday

---

Abstract

Complexes [Pt(C_6F_5)(bzq)L] (bzq = 7,8-benzoquinolinate; L = 8-hydroxyquinoline, hqH (**1**); 2-methyl-8-hydroxyquinoline, hqH' (**2**)) have been prepared by replacing the labile acetone ligand in the starting material [Pt(C_6F_5)(bzq)(Me_2CO)]. The ^{1}H NMR spectra of **1** and **2** show that the signals attributable to the hydroxyl proton of the hqH or hqH' ligands are displaced downfield 2.64 ppm for **1** and 2.74 ppm for **2** with respect to the respective free ligands. Moreover, in both complexes the signals present platinum satellites with *J*(Pt,H) coupling constant of 67.0 Hz for **1** and 80.6 Hz for **2**. All these features are indicative of the existence of Pt···H–O hydrogen bonds in solution for these complexes**.** The structures of complexes **1** and **2** have been established by an X-ray diffraction study and allow us to confirm the existence of these interactions in the solid state too. Thus, in both cases the hydroxyl hydrogen atom is pointing toward the metal center and the measured geometric parameters involving this hydrogen are: Pt–H = 2.09(4) Å, O–H = 0.94(4) Å, Pt–H–O 162(4)º, for **1**, and Pt–H = 2.10(4) Å, O–H = 0.91(4) Å, Pt–H–O 162(4)º, for **2**, all of which are fully compatible with a hydrogen bond system. Complexes **1** and **2** and the analogues [Pt(C_6F_5)$_3$(hqH)]$^-$ (**A**) and [Pt(C_6F_5)$_3$(hqH')]$^-$ (**B**), prepared some time ago in our laboratory and also showing Pt···H–O hydrogen bonds, have been the object of theoretical calculations in order to obtain better insight into the Pt···H interactions. Their DFT calculated structures show excellent agreement with the X-ray determined ones (**1**, **2** and **B**). Topological analyses of the electron density function (ρ(**r**)) have been performed on the four complexes according to

Bader's *Atoms In Molecules* theory. These analyses reveal a bond path that relates the platinum atom and the hydroxyl hydrogen atom, as well as the corresponding bond critical points. The values of the Laplacian $\nabla^2\rho(\mathbf{r})$ and local energy density $H(\mathbf{r})$ indicate that these are closed shell, electrostatic interactions, but with *partial covalence*.

The deprotonation of the OH fragment in **1** and **2** with BuLi leads to the formation of the unexpected trinuclear complexes $(NBu_4)[Li\{Pt(C_6F_5)(bzq)(L)\}_2]$ (L = hq (**3**), hq' (**4**)). The X-ray structures of these have shown a change in the coordination of the deprotonated hq and hq', which are now bonded to the Pt atoms through their O atoms, and which are bridging the Pt and Li metal atoms.

Introduction

The existence of interactions between metal centers and hydrogen atoms attached to main group elements (especially C, N and O) has been recognised since the early 1980s.[1-3] The first of these types of interactions to be studied and understood were the “agostic” interactions.[1,4] In these, the metal center acts as a Lewis acid, generally receiving electron density from a C–H bond and resulting in a 3-center–2-electron (3c-2e) bond system. The three centers are the metal and the C and H atoms, and the two electrons are those in the C–H bond. An empty orbital of the metal is involved to house the donated electron density. A characteristic of agostic interactions is the upfield displacement in the ^{1}H NMR spectra of the signal of the hydrogen involved.

In the second type of M···H interactions a transition metal atom is acting as a proton acceptor in a formally hydrogen bonding interaction. Although some early reports on IR studies in solution[5] mention the possibility of metal centers being involved in hydrogen bridging, these M···H–X systems have been recognised and understood from the early 1990s and now they are well established.[2,3,6-10] They are substantially similar to “classic” hydrogen bonds, that is, the metal atom is the Lewis base that has a filled orbital with an electron pair that can interact with an electropositive hydrogen atom. Using a molecular orbital method language, the electron pair is donated to create a 3-center–4-electron (3c-4e) system. These hydrogen bonds therefore are favored by electron rich metals such as late transition metals, especially in low oxidation states. Pt(II) complexes have been found to be particularly suited to this interaction due to its planar nature and the electron pair housed in the $5d_{z^2}$ orbital, available to participate in the Pt···H–X 3c-4e system of the hydrogen bond. The signal of the proton involved in the M···H–X hydrogen bonding moves downfield in the ^{1}H NMR spectra, which is a common feature of all hydrogen bond systems.

The terms “anagostic”[1,11] or “pregostic”[12] have been used to refer to M···H–C interactions which clearly do not fit the “agostic" definition. Structurally and spectroscopically, they are more similar to the hydrogen bonding M···H–X systems, but given the low ability of the C atom to act as a proton donor in a C–H fragment, their bonding description is still unclear. Nevertheless, some theoretical studies would seem to indicate that the d_{z^2} orbital in d^8 square planar complexes is not involved in the interaction in certain cases.[11]

While a fair amount of structural solid state studies have been carried out by X-ray or neutron diffraction,[9,13,14] there is relatively scarce evidence of the existence of M···H hydrogen bridging in solution achieved through simultaneous observation of the downfield on the H signal and M-H coupling.[6,15-17] The highest value of a *J*(Pt,H) coupling constant (180 Hz) has been found in complex [PtBr{1-$C_{10}H_6(NMe_2)$-8-*C,N*}{1-$C_{10}H_6(NHMe_2)$-8-*C,H*}].[15] In this example, the hydrogen involved is very acidic due to the ammonic nature of the N donor fragment. Smaller values of the coupling constants have been reported for amino donor fragments, such as in [Pt(C_6H_3-2,6E_2)(8-acetylaminequinoline)]$^+$ (E = PPh_2, *J*(Pt,H) = 55 Hz; NMe_2, *J*(Pt,H) = 33 Hz).[16] Intermediate values of *J*(Pt,H) (69 and 88 Hz, respectively) have been found in anionic complexes [Pt(C_6F_5)$_3$(hqH)]$^-$ (**A**) and [Pt(C_6F_5)$_3$(hqH')]$^-$ (**B**, see Scheme 1),[6] which contain the 8-hydroxyquinoline (hqH) or 2-methyl-8-hydroxyquinoline (hqH') ligands, with a O-H donor fragment. Usually, with even less acidic C-H protons such as the contained in the 7,8-benzo[*h*]quinoline (bzqH) ligand of complex [Pt(C_6F_5)$_3$(bzqH)]$^-$[6], the value observed for the Pt-H coupling constant is even lower (22 Hz). Nevertheless, higher *J*(Pt,H) can be observed when the C-H group is strongly oriented toward the Pt atoms by the geometry of the ligand. This is the case of the complexes [Pt(Me_3Si-BAM)Me_2] and [Pt(Me_3Si-BAM)Ph_2] (BAM = bis(7-azaindol-1-yl)methane)[17] for which values of 61.0 Hz and 44.1 Hz respectively have been reported. Theoretical studies have also been carried on these complexes containing M···H–X hydrogen bonds.[2,9,11,18-21] They indicate that most systems show an important electrostatic contribution interaction, as in "classic" hydrogen bonds. Nevertheless, it has been suggested that the importance of a covalent contribution increases as the M···H distance shortens and thus the strength of the interaction increases.[2,11]

Recently, the first crystallographic evidence by neutron difraction of intermolecular hydrogen bonding involving a d^8 metal center and a hydrogen atom of a crystallization water molecule has been reported in the complex *trans*-[$PtCl_2(NH_3)$(N-Glycine)].[9] The structure also presents an intramolecular Pt···H–N interaction. Interestingly, theoretical studies of this system conclude that dispersion forces constitute the main component of the intermolecular Pt···H-O contact[9,18,20] and also support the persistence of this interaction in solution.[19,20]

In the course of previous research, we prepared anionic *tris* pentafluorophenyl Pt(II) complexes containing Pt···H–X (X = O, C) hydrogen bonds.[6] In this paper we have explored the use of neutral Pt(II) pentafluorophenyl complexes which also contain the 7,8-benzoquinolate chelate planar ligand as precursors for complexes containing Pt···H–O hydrogen bonding with success. The overall charge in the complex and the different steric

requirements of the ligands surrounding the metal center might influence the characteristics of the Pt···H interactions, which have been studied both in the solid state (X-ray) and in solution (NMR). Moreover, theoretical calculations have been performed in order to obtain a greater insight into the nature of the Pt···H interaction. For comparative purposes, studies on **A** and **B**, a couple of similar complexes previously prepared in our laboratory[6] (see Scheme 1), have also been included in this paper. The study of the reactivity of the Pt···H complexes toward hydrogen abstractors has resulted in unexpected polynuclear complexes which have also been fully characterized.

Synthesis and characterization of the complexes [Pt(C_6F_5)(bzq)L] {L = hqH, 8-hydroxyquinoline (1); L = hqH', 2-methyl-8-hydroxyquinoline (2)}

Complex [Pt(C_6F_5)(bzq)(Me_2CO)] (bzq = 7,8-benzoquinolinate) has proven to be a suitable precursor for the preparation of complexes [Pt(C_6F_5)(bzq)L] due to the fact that the acetone group is easily replaced with other L ligands.[22,23] Thus, the addition of equimolecular amounts of 8-hydroxyquinoline (hqH) or 2-methyl-8-hydroxyquinoline (hqH') to dichloromethane solutions of [Pt(C_6F_5)(bzq)(Me_2CO)] under protective Ar atmosphere and at 273 K allows to obtain after 15 minutes of stirring the corresponding complexes [Pt(C_6F_5)(bzq)L] {L = hqH (**1**), hqH' (**2**), see Scheme 1} as yellow solids which precipitate after partial evaporation of the solvent.

The IR spectra of complexes **1** and **2** confirm the replacement of the acetone in the starting material, since the ν_{CO} vibration band corresponding to this ligand which appears at 1669 cm^{-1} is no longer present, and bands assignable to the hqH and hqH' ligands can now be observed (see Experimental).

The ^{19}F NMR spectra of **1** and **2** present the same pattern of five signals, indicating that all the five fluorine atoms of the C_6F_5 ligands are inequivalent. The two *ortho*-F appear at lower field with platinum satellites. At higher field, one signal for the *para*-F and one for each of the *meta*-F can be observed. The inequivalence of the fluorine atoms in analogous positions of the pentafluorophenyl rings indicates the difficulty of this group to rotate around the Pt–C_{ipso}, probably due to the bulkiness and rigidity of the neighboring chelating bzq ligand.

The ^1H NMR spectra of these complexes are more interesting. Figures 1 and 2 show these spectra for complexes **1** and **2** respectively. They show the signals corresponding to the hydroxyquinoline ligands in the aromatic area besides the ones attributed to the bzq ligand

with the expected relative intensity. Moreover, in the case of complex **2**, a singlet signal corresponding to the methylic hydrogen atoms appears at 3.40 ppm. However, the most striking feature of these spectra is the presence at low field of a sharp signal with platinum satellites assignable to the hydroxylic proton of the hydroxyquinoline ligands. This signal appears at 10.92 ppm in **1**, with a coupling constant *J*(Pt,H) = 67.0 Hz, and at 10.99 ppm in **2**, with a coupling constant *J*(Pt,H) = 80.6 Hz. The downfield displacement of these signals with respect to the free ligands[6] (2.64 ppm for **1** and 2.74 ppm for **2**) and, most importantly, the existence of the Pt-H coupling, accounts for the existence of the Pt···H–O hydrogen bond in solution for complexes **1** and **2**. Similar Pt-H coupling constants have been reported for the related complexes $[Pt(C_6F_5)_3(hqH)]^-$ (**A**) and $[Pt(C_6F_5)_3(hqH')]^-$ (**B**),[6] (69 Hz, and 88 Hz, respectively, see Table 1). Nevertheless, the chemical displacement of the signal of the hydrogen involved in the interaction is greater (3.70 ppm and 4.09 ppm respectively).

The close vicinity of the platinum center and the hydroxylic hydrogen atom is also manifest in another magnetic property of the latter, the relaxation rate.[24] Thus the I = 1/2 platinum isotope in the ^{195}Pt···H–O isotopomer makes an additional contribution to the relaxation rate of the corresponding hydrogen atom. As a consequence, the $T_{1(min)}$ values measured for the satellite signals (which are due to the ^{195}Pt···H–O isotopomer) are slightly shorter than those measured for the central signal (which belong to the rest of the platinum isotopomers).[25] In CD_2Cl_2 as solvent, the measured $T_{1(min)}$ values for the central singlet are 1.55 (**1**) and 1.45 (**2**) s, whereas those measured for the doublet corresponding to the ^{195}Pt isotopomers are 1.45 (**1**) and 1.28 (**2**) s. All those magnetic parameters are summarized in Table 1

The structures of complexes **1** and **2** have been established by single crystal X-ray diffraction studies. Figures 3 and 4 show views of the structures of **1** and **2** respectively, and Table 2 lists a selection of relevant bond distances and angles for both complexes. As expected, **1** and **2** are square planar complexes in which the pentafluorophenyl ligand is located *trans* to the nitrogen donor atom of the cyclometalated bzq ligand, as has previously been found in complexes with the formula $[Pt(C_6F_5)(bzq)L]$.[23] In both structures, the bzq planes are coplanar to the Pt basal square planes (dihedral angle 3.4(1)º for **1** and 4.4(1)º for **2**), while hqH and C_6F_5 ligands are almost perpendicular to the latter (dihedral angles are 80.7(1)º and 78.5(1)º respectively for **1** and 84.0(1)º and 84.6(1)º for **2**). With these dispositions, the OH fragments of the hqH and hqH' ligands have optimal orientations for the hydrogen atoms to establish interactions with the Pt centers. It is noteworthy that the quality

of the X-ray diffraction data collected has allowed, in both structures, to find and refine the position of these hydrogen atoms (H(1)) without restraints, and that from all the possible orientations, the hydrogen atoms are pointing toward the metal centers. Thus, the measured geometric parameters involving H(1) are: Pt–H(1) = 2.09(4) Å, O–H(1) = 0.94(4) Å, Pt–H(1)–O 162(4)º for **1** and Pt–H(1) = 2.10(4) Å, O–H(1) = 0.91(4) Å, Pt–H(1)–O 162(4)º for **2**. If the O–H(1) distances are normalized to 0.993,[26] then the Pt–H(1) distances are 2.04 Å in **1** and 2.07 Å in **2**. In any case, these parameters are fully consistent with the existence of Pt···H(1)–O hydrogen bond systems in the solid state,[2,3] in fact, the Pt–H(1) distances found in **1** and **2** (2.09(4) Å, 2.10(4) Å) are the shortest reported for this kind of hydrogen bonding. Slightly longer distances have been found in complexes [PtBr{1-$C_{10}H_6(NMe_2)$-8-*C,N*}{1-$C_{10}H_6(NHMe_2)$-8-*C,H*}] (2.11(5) Å),[15] **B** (2.19 Å),[6] and [Pt(C_6H_3-2,6(PPh_2)$_2$)(8-acetylaminequinoline)](CF_3SO_3) (2.2(1) Å).[16] Nevertheless, fine comparisons of the Pt–H distances must be performed with caution due to the inherent uncertainty of the location of the hydrogen atoms from single crystal X-ray diffraction studies. As expected, the Pt–H distance found in the structure of *trans*-[$PtCl_2(NH_3)$(N-Glycine)]·H_2O, determined by neutron diffraction,[9] is much longer (2.885(3) Å), since it arises from an intermolecular interaction between the Pt center and a crystallization water molecule.

Computational studies.

The molecular structures of the complexes **1**, **2**, **A** and **B** have been optimized by DFT methods, at the M06 level of theory (see Experimental Section for further details). A comparison of the most relevant structural parameters of **1**, **1-DFT**, **2**, **2-DFT**, **A-DFT**, **B** and **B-DFT** is included in Table 3. Views of the optimized structures for **1-DFT**, **2-DFT**, **A-DFT** and **B-DFT** are included in Figure 5. The geometries of **1-DFT** and **2-DFT** are consistent with the structures found by X-ray diffraction (see Figures S1 and S2, Supporting Information). In agreement with the existence of a Pt···H short contact, the Pt···H(1) distance is 2.18 Å, the H(1)-O bond length is 0.98 Å and the Pt–H(1)–O is 153.6º for **1-DFT**, while for **2-DFT** the calculated parameters are 2.15, 0.98 Å and 152.4º respectively. These Pt-H distances are slightly longer than those determined crystallographically and support 4e-3c type interactions. The optimized geometry of **B** (**B-DFT**) is also consistent with the X-ray determined structure.[6] It also shows that the hydrogen atom of the hydroxyl fragment is oriented toward the platinum atom resulting in a very short distance of 2.11 Å (2.19 Å, X-ray), and all the Pt···H–O structural parameters are consistent with a hydrogen bonding 4e-3c

type interaction (see Table 3). The optimized geometry of the analogous **A** (**A-DFT**) is very similar, thus supporting the existence of a Pt···H–O hydrogen bonding system.

The coherence observed for these structures has led us to investigate the Pt···H contacts in more detail through DFT methods. Topological analyses of the electron density function ($\rho(\mathbf{r})$) obtained for **1-DFT**, **2-DFT**, **A-DFT** and **B-DFT** have been performed. According to Bader's *Atoms In Molecules* theory,[27-31] the critical points (CP) in the $\rho(\mathbf{r})$ function are the points in space at which the first derivatives of the function vanish (*i.e.*, each individual derivative in the gradient operator is zero). CPs indicate chemically meaningful points and are classified according to their rank and signature. The rank is the number of non-zero curvatures of the electron density $\rho(\mathbf{r})$ at the CP, whereas the signature is the algebraic sum of the signs of the curvatures. For example, CPs of the (3,-3) type are indicative of the nuclear positions, whereas CPs of the (3,-1) type are evidences of chemical bonds. Complementarily, a bond path (BP) is a single line of maximum electron density linking the nuclei of two chemically-bonded atoms. A BP is an indicator of chemical bonding of all kinds; weak, strong, closed-shell, and open-shell interactions. The point on the BP with the lowest electron density value (minimum along the path) is the bond critical point (BCP).

The analyses of the electron density functions in **1-DFT**, **2-DFT**, **A-DFT** and **B-DFT** reveal a bond path relating the platinum atom and the hydroxyl hydrogen atom in all four cases, as well as the corresponding bond critical points. Observation of the properties of the electron density at the referred CPs sheds light onto the nature and properties of the discussed contacts. Cremer *et al.* have stated that to provide a thorough description of the CP, electrostatic and also energetic aspects must be considered.[32] Thus, a negative value of $\nabla^2\rho(\mathbf{r})$ indicates a covalent (shared electron) interaction, while a positive value is associated with a closed-shell, electrostatic interaction. Complementarily, a negative value of the local energy density function $H(\mathbf{r})$ corresponds to partial covalence, while a positive $H(\mathbf{r})$ indicates a purely closed-shell, electrostatic interaction.[11,27,28]

The results of our study on the referred BCPs found for **1-DFT**, **2-DFT**, **A-DFT** and **B-DFT** are shown in Table 4. The electron density $\rho(\mathbf{r})$ at a BCP correlates with the strength of an atomic interaction. For a typical C–C covalent bond the value of $\rho(\mathbf{r})$ is about 1.7 au.[33] For conventional purely organic hydrogen bonding values of between 0.0123 and 0.0276 au have been reported.[33] Bergès *et al.*[20] have found $\rho(\mathbf{r})$ values of about 0.020 au for the intermolecular Pt···H interactions between d^8 square planar Pt(II) complexes and the water molecules discussed above. In the complexes studied in this paper, the values of $\rho(\mathbf{r})$ are

higher, ranging from 0.034 to 0.039, and also higher that those reported by Oldfield and coworkers[11] for d^8 square planar complexes containing intramolecular M···H–X (X = C, N) interactions (range 0.012-0.025), or by Pérez-Prieto and coworkers[34] in intramolecular M···H–C (M = Pd, Ag, Mo) interactions (range 0.019-0.034). Thus, these values of $\rho(\mathbf{r})$ at the BCP seem to indicate a significant Pt···H interaction in the complexes studied here. According to the $E_{cont} = 1/2V(\mathbf{r}_{CP})$ relationship, the energies of the hydrogen bonds can be estimated to lay between -8.1 and -10.0 Kcal mol^{-1}.[35,36]

With respect to the sign of the Laplacian $\nabla^2\rho(\mathbf{r})$, in all four cases their values are positive (see Table 4), thus indicating closed-shell, electrostatic interactions. This same result is also observed in conventional organic hydrogen bonds,[33] in the referred Pt(II)··H–OH interactions[20,21] or in other studies on M···H–X systems[11,34] Nevertheless, and as stated before,[11,33,34] considering the values and signs of $\nabla^2\rho(\mathbf{r})$ and $H(\mathbf{r})$ together allows a better understanding of these interactions. Thus, in the four examples studied here, all the $H(\mathbf{r})$ values are negative (see Table 4), which means that the Pt···H–O hydrogen bonds have *partial covalence*. Analogous results have been found in other pregostic or hydrogen bonded M···H–X interactions,[11,34] in contrast to conventional organic hydrogen bond systems for which positive values of $H(\mathbf{r})$ are always calculated, and thus no covalent component is deduced in the interaction.[33]

It has been observed that a more negative value of $H(\mathbf{r})$ is related to the decrease in the distance between the interacting atoms, both in certain specific organic hydrogen bonding systems[33,37] and in other non-bonded interactions.[38] In these specific hydrogen bonding systems the donor or proton acceptors are ylides[37] or organic acids,[33] and when known, the X···H distances have been shown to be very short. These “special” hydrogen bonds are sometimes termed “Low Barrier Hydrogen Bonds” (LBHB) and are postulated as transition states in several organic and enzyme catalytic events.[33,37] The values of $H(\mathbf{r})$ reported for the complexes investigated here are the most negative ones calculated for M···H–X interactions[11,34] (see Table 4), and certainly, the Pt–H distances calculated or measured by X ray (complexes **1** and **B**, see Table 3), are among the shortest reported for this kind of complexes[6,15,16]

Some authors have stated that the shorter the Pt···H contact, the more negative the value of $H(\mathbf{r})$ is and the greater the downfield displacement of the interacting hydrogen is in the ^{1}H NMR spectra.[11] In the case of the four complexes studied here, the calculated or measured

values of the Pt–H distances are very similar, ranging from 2.09 Å to 2.19 Å (see Table 1). Nevertheless, the value of the downfield displacement of the signal of the interacting hydrogen in the ^{1}H NMR with respect to the free ligand is significantly greater for the complexes **A** and **B** (3.70 and 4.09 ppm, respectively) than it is for **1** and **2** (2.64 and 2.74 ppm, respectively). Thus, in these cases the Pt–H distance would seem to be not the only factor determining the magnitude of the downfield displacement in the signal of the hydrogen involved in the interaction.

NBO analyses have been performed for **1-DFT**, **2-DFT**, **A-DFT** and **B-DFT** (see Table S7, Supporting Information). As a result of the anionic nature of the latter pair of complexes, the atomic charges on the platinum centers of **1-DFT** and **2-DFT** (+0.23 and +0.22) are higher than those in **A-DFT** and **B-DFT** (+0.11 and +0.09). This trend is also observed in the Mulliken charges (+0.09 in **1-DFT**, +0.06 in **2-DFT**, -0.09 in **A-DFT** and -0.11 in **B-DFT**). Oppositely, the calculated charges on the hydroxyl hydrogen and on the oxygen atoms are almost identical in the series of four cases under study (average values are +0.52 for the hydrogen and -0.70 for the oxygen atoms according to NBO, and +0.41 for the hydrogen and -0.56 for the oxygen atoms according to Mulliken). The ^{1}H chemical shifts of the free quinoline and quinaldine molecules and of the **1-DFT**, **2-DFT**, **A-DFT** and **B-DFT** complexes have also been calculated by DFT methods and compared to the experimental values (see Table 1). The calculated shifts for the hydroxylic hydrogen atoms in the organic substrates (7.69 and 8.06 ppm respectively) and in the four organometallic complexes (10.71, 10.95, 11.95, and 12.07 ppm respectively) are in a good agreement with the experimental ones, both from a qualitative and quantitative point of view (see Table 1). Remarkably, the computed shifts reproduce the experimentally observed downfield delta shifts upon formation of the Pt···H interactions, and predict higher deshieldings for the hydroxylic proton of the aromatic ligands when coordinated to the anionic $[Pt(C_6F_5)_3]^-$ fragment (+4.26 for **A-DFT** and +4.01 for **B-DFT)**, than when coordinated to the neutral $[Pt(C_6F_5)(bzq)]$ (+3.02 for **1-DFT** and +2.89 for **2-DFT)**. The sum of these observations suggests that the strengths of the Pt···H interactions and the extent of the downfield shifts of the hydroxylic hydrogen atoms participating in the platinum-hydrogen contacts are determined not only by the short values of the Pt···H distances but also by the charges of the platinum centers in these sets of compounds. According to this, a more negative charge on the platinum center would favor stronger hydrogen bonds as well as more downfield chemical ^{1}H shifts in the resulting complexes.

Reactivity of complexes 1 and 2 toward bases.

The hydrogen bridging M···H interactions have been described as the first step in processes of protonation of the metal and possible migration of the proton to a ligand with elimination of the protonated ligand.[2] For example, complex $[Pt(C_6F_5)_3(bzqH)]^-$, which shows evidence of the existence of the Pt···H interaction through Pt-H coupling in its ^1H NMR spectrum (see above), undergoes cyclometalation of the bzq ligand with elimination of C_6F_5H when is refluxed in 1,2-dichloroethane for three hours, giving rise to $[Pt(C_6F_5)_2(bzq)]$.[39] Furthermore, the preparation of the starting material $[Pt(C_6F_5)(bzq)(Me_2CO)]$ is achieved *via* this pathway, with coordination of the Hbzq ligand to the platinum center in reflux of acetone solutions of *cis*-$[Pt(C_6F_5)_2(THF)_2]$[23] However, complexes **1** and **2** do not undergo a similar process, with the cyclometallation of the hqH ligand, when their solutions are refluxed for several hours, even in relatively high boiling point solvents such as 1,2-dichloroethane.

Since the "internal" deprotonation, chelation, and corresponding formation of C_6F_5H do not take place, we tested the acidity of the OH hydrogen of the hydroxyquinoline ligands in **1** and **2** toward several "external" deprotonating reagents. Successful abstraction of the proton from the hydroxyl fragment should afford a monoanionic complex with a formally negative oxygen atom that could be used as a building block for preparing compounds of higher nuclearity, for example by reaction with acidic metals such as Ag(I), Au(I), or Tl(I). Although no deprotonation was achieved using KOH, $K(Me_3CO)$, or 1,8-bis(dimethylamino)naphthalene (proton sponge), the reactions with BuLi led to unexpected results. Thus, the treatment of THF solutions of **1** or **2** with equimolar amounts of BuLi for 1h at 198 K and the subsequent room temperature addition of $(NBu_4)ClO_4$ afforded, after work-up, two yellow solids in good yields (see Experimental for details). The ^1H NMR spectra of these yellow solids do indeed show the absence of the downfield signal corresponding to the OH hydrogen atoms of the hydroxyquinoline ligands, with signals corresponding to the other protons of these and the bzq ligands in 1:1 ratio. They also show signals for NBu_4^+, but with half the intensity expected for a $(NBu_4)[Pt(C_6F_5)(bzq)(hq)]$ or $(NBu_4)[Pt(C_6F_5)(bzq)(hq')]$ stoichiometry. Their ^{19}F NMR spectra show signals for five fluorine atoms in the region and intensity expected.

The nature of the yellow solids could only be established when their structures were determined by single crystal X-ray diffraction. These studies concluded that the stoichiometry of the prepared complexes was in fact $(NBu_4)[Li\{Pt(C_6F_5)(bzq)(L)\}_2]$ (L = hq (**3**), hq' (**4**)). For complex **4**, two sets of different crystals have been obtained, corresponding to two

pseudopolymorphs,[40] one triclinic (*P*-1) which incorporates two CH_2Cl_2 solvent molecules in the asymmetric unit, and one monoclinic ($P2_1/n$) with one CH_2Cl_2 molecule. The structural parameters for both pseudopolymorphs are very similar and will be denoted **4a** and **4b** respectively. Figures 6 and 7 show views of the complexes **3** and **4a**, and Tables 5 and 6 list a selection of their relevant bond distances and angles. A figure, table of selected bond distances and angles, and crystallographic data for **4b** are included as Supporting Information.

Complexes **3**, **4a** and **4b** are isostructural, with the obvious difference of the methyl substituent on the 2-methyl-hydroxyquinolinate ligand, and small differences mainly in the conformation of the pentafluorophenyl and hydroxyquiolinate ligands that probably can be accounted by the flexibility of the molecules in the crystalline environment.[41] The three complexes are trinuclear, with two "Pt(C_6F_5)(bzq)(L)" subunits bridged by a lithium atom. The most remarkable feature of the structures is the change of coordination mode of the hydroxyquinolinate ligands. Thus, the deprotonation of the hydroxyl group and the presence of the lithium atom cause a change in the bond between the platinum center and the hydroxyquinolinate ligand, which now is established through a Pt–O bond. This change in the donor atom allows the oxygen atom to act as a bridge between the two metals. Furthermore, in this way, the lithium also coordinates to the now available nitrogen atom and is able to reach the four coordination with a distorted tetrahedral environment. A few lithium hydroxyquinolate complexes have been previously described in the literature, which are tetrametallic or hexametallic with cyclic structures in which the Li atoms are bridged by three oxygen atoms of the hq ligand and only the fourth coordination position is occupied by a N atom.[42,43]

The two Pt square planes are nearly coplanar, in a disposition that is probably optimal to reduce the steric repulsions of the bulky benzoquinolinate chelate ligands. Furthermore, the two bzq planes are separated about 3.4 Å, a distance that could indicate the existence of π···π interactions of the planar aromatic rings in a similar fashion to that previously reported for other complexes containing the bzq ligand.[23,44-46]

Conclusion

The combination of the 8-hydroquinoline type ligands and square planar Pt(II) complexes has shown to be a good way to design complexes which contain Pt···H–O hydrogen bonds. Thus, **1** and **2** are examples of complexes exhibiting this kind of interaction both in solution and in the solid state. Their ^{1}H NMR spectra show the two expected features that prove the interactions: a) downfield displacements of the signals of the involved

hydrogen atoms and, even more conclusive, b) the existence of Pt-H couplings with values of *J* of appreciable magnitude, indeed some of the greatest reported so far. Moreover, the X-ray structures of **1** and **2** have revealed that the structural parameters of the fragment Pt–H–O are typical of a hydrogen bonding system. In particular, the Pt–H distances are very short, 2.09(4) and 2.10(4) Å, and indicate a quite strong interaction. The *Atoms in Molecules* study on complexes **1** and **2**, and also on the related complexes **A** and **B** (see Scheme 1), confirms the existence of interactions between the metal centers and the OH hydrogen atoms of electrostatic nature but with a *partial covalence*. This description is derived from the values of the Laplacian $\nabla^2\rho(\mathbf{r})$ and the local energy density function $H(\mathbf{r})$ calculated for the Pt···H–O systems. In particular, besides their sign, the magnitude of the value of $H(\mathbf{r})$ has also been directly related with the distance Pt–H, which correlates well with the observations for **1**, **2**, **A** and **B**, and with the magnitude of the downfield displacement of the ^{1}H NMR signal of the hydrogen.[11] Nevertheless, in the cases studied in this paper the magnitude of this NMR displacement seems to be also related to the difference of charge between the Pt and the H, as suggested by NBO analyses of the complexes.

Several reagents have been tested as deprotonating agents for the hydroxyl OH in **1** and **2**, and only BuLi has proved to work properly. Nevertheless, the process evolves toward the formation of unexpected trinuclear Pt_2Li complexes, in which the coordination mode of the deprotonated 8-hydroquinolinate type ligands changes. The hq and hq' ligands are now O-coordinated to the Pt atom, and O,N- chelate to the Li atom, in such a way that the Li is tetracoordinated and bridges two platinum subunits.

Experimental

General Comments. Literature methods were used to prepare the starting material $[Pt(C_6F_5)(bzq)(Me_2CO)]$.[22] Elemental analyses were carried out with a Perkin-Elmer 2400 CHNS analyzer. IR spectra were recorded on a Perkin-Elmer Spectrum 100 FT-IR spectrometer (ATR in the range 250-4000 cm^{-1}). Mass spectrometry was performed with the Microflex matrix-assisted laser desorption ionization-time-of-flight (MALDI-TOF) Bruker or an Autoflex III MALDI-TOF Bruker instruments. NMR spectra in solution were recorded at 298K on Bruker Avance 400 spectrometer with $SiMe_4$ and $CFCl_3$ as external references for ^{1}H, ^{13}C and ^{19}F. The signal attributions and coupling constant assessment was made on the basis of a multinuclear NMR analysis of each compound including, besides ID spectra, ^{1}H COSY, ^{1}H-^{13}C HMQC, ^{1}H-^{13}C HMBC and APT.

Preparation of [Pt(C_6F_5)(bzq)(8-hydroxyquinoline)] (1). To a solution of [Pt(bzq)(C_6F_5)(Me_2CO)] (0.150 g, 0.251 mmol) in CH_2Cl_2 (20 mL) at 273 K and under Ar atmosphere, 0.251 mmol (0.036 g) of 8-hydroxyquinoline were added. After 15 min of stirring the solution was concentrated until *ca.* 2 mL. The yellow precipitate which appeared was filtered off, washed with *n*-hexane (10 mL) and air dried. Yield 0.148 g (0.216 mmol), 86% yield. IR υ = 2946 (w, υ_{OH}), 1576 (vw), 1497 (m), 1450 (m), 1438 (m), 1208 (w), 1059 (m), 952 (s), 801 (m, C_6F_5, X-sensitive vibr.)[47] cm^{-1}. ^{1}H NMR (400.132 MHz, CD_2Cl_2, 298 K): δ = 10.92 (1H, s, *J*(H,Pt) = 67.0 Hz, H; hqH'-OH), 9.62 (1H, d, ^3J(H2,H3) = 5.1 Hz, ^3J(H2,Pt) = 23.4 Hz, H2, see Scheme 2 for the hydrogen and carbon numbering scheme), 8.44 (1H, dd, ^3J(H4,H3) = 8.4 Hz, ^4J(H4,H2) = 1.6 Hz, H4), 8.37 (1H, dd, ^3J(H17,H16) = 8.1 Hz, ^4J(H17,H15) = 1.3 Hz, H17), 7.85 (1H, d, ^3J(H6,H5) = 8.8 Hz, H6), 7.65 (1H, d, ^3J(H6,H5) = 8.8 Hz, H5), 7.64 (1H, dd, ^3J(H7,H8) = 7.9 Hz, ^4J(H7,H9) = 0.8 Hz, H7), 7.62 (1H, t, ^3J(H19,H20) = ^3J(H19,H18) = 7.7 Hz, H19), 7.60-7.52 (3H, m, overlapped signals of H15, H18 and H3), 7.39 (1H, dd, ^3J(H8,H9) = 7.9 Hz, ^3J(H8,H7) = 7.9 Hz, H8), 7.33 (1H, dd, ^3J(H20,H19) = 7.7 Hz, ^4J(H20,H18) = 1.5 Hz, H20), 7.29 (1H, dd, ^3J(H16,H17) = 8.1 Hz, ^3J(H16,H15) = 5.2 Hz, H16), 7.00 (1H, d, ^3J(H9,H8) = 7.8 Hz, ^3J(H9,Pt) = 62.5 Hz, H9) ppm. ^{19}F NMR (376.479 MHz, CD_2Cl_2, 298 K): δ = –117.9 (*o*-F, m, ^3J(F,Pt) = 515 Hz), -121.2 (*o*-F, m, ^3J(F,Pt) = 444 Hz), -163.3 (*p*-F, t), -164.5 (*m*-F, br m), -165.0(*m*-F, br m) ppm. ^{13}C{^{1}H} NMR (100.624 MHz, CD_2Cl_2, 298 K): δ = 155.4 (s, C12), 153.2 (s, C2), 152.2 (s, C21), 146.2 (s, C15), 142.7 (s, C11), 140.3 (s, C4), 138.6 (s, C17), 136.4 (s, C22), 135.9 (s, C10), 134.7 (s, ^2J(C,Pt) = 114 Hz, C9), 134.2 (s, C14), 132.3 (s, C23), 130.2 (s, C5), 129.8 (s, C8), 129.4 (s, C19), 123.5 (s, C6), 123.2 (s, C7), 122.2 (s, C16), 122.0 (s, C18), 120.3 (s, C3), 117.3 (s, C20) ppm. Mass spectra MALDI+ DCTB: *m/z* = 517.0 [Pt($C_{13}H_8N$)(C_9H_7NO)], 684.0 [Pt($C_{13}H_8N$)(C_6F_5)(C_9H_6NOH)-H]$^+$. Elemental analysis calcd (%) for $C_{28}H_{15}F_5N_2OPt$: C 49.06, H 2.21, N 4.09; found: C 48.72, H 2.25, N 4.02.

Preparation of [Pt(C_6F_5)(bzq)(2-methyl-8-hydroxyquinoline)] (2). To a solution of [Pt(bzq)(C_6F_5)(Me_2CO)] (0.150 g, 0.251 mmol) in CH_2Cl_2 (20 mL) at 273 K and under Ar atmosphere, 0.251 mmol (0.040 g) of 2-methyl-8-hydroxyquinoline were added. After 15 min of stirring the solution was concentrated until *ca.* 2 mL. The yellow precipitate which appeared was filtered off, washed with *n*-hexane (10 mL) and air dried. Yield 0.154 g (0.220 mmol), 88% yield. IR υ = 2938 (w, υ_{OH}), 1569 (w), 1504 (m), 1450 (m), 1438 (m), 1258 (m), 1060 (m), 955 (s), 797 (m, C_6F_5, X-sensitive vibr.)[47] cm^{-1}. ^{1}H NMR (400.132 MHz, CD_2Cl_2, 298 K): δ = 10.99 (1H, s, *J*(H,Pt) = 80.6 Hz, H; hqH'-OH), 8.42 (1H, dd, ^3J(H4,H3) = 8.1 Hz,

^4J(H4,H2) = 1.2 Hz, H4, see Scheme 2 for the hydrogen and carbon numbering scheme), 8.27 (1H, d, ^3J(H17,H16) = 8.5 Hz, H17), 8.10 (1H, dd, ^3J(H2,H3) = 5.3 Hz, ^4J(H2,H4) = 1.2 Hz, ^3J(H2,Pt) = 19.4 Hz, H2), 7.88 (1H, d, ^3J(H6,H5) = 8.8 Hz, H6), 7.67 (1H, d, ^3J(H5,H6) = 8.8 Hz, H5), 7.66 (1H, dd, ^3J(H7,H8) = 7.9 Hz, ^4J(H7,H9) = 0.7 Hz, H7), 7.52 (1H, t, ^3J(H19,H20) = ^3J(H19,H18) = 7.8 Hz, H19), 7.44-7.38 (3H, m, overlapped signals of H18,H8 and H3), 7.42 (1H, d, ^3J(H16,H17) = 8.5 Hz, H16), 7.28 (1H, dd, ^3J(H20,H19) = 7.8 Hz, ^4J(H20,H18) = 1.6 Hz, H20), 7.02 (1H, d, ^3J(H9,H8) = 7.2 Hz, ^3J(H,Pt) = 62.0 Hz, H9), 3.40 (3H,s, H; hqH'-CH_3) ppm. ^{19}F NMR (376.479 MHz, CD_2Cl_2, 298 K): δ = –117.8 (*o*-F, m, ^3J(F,Pt) = 435 Hz), -118.5 (*o*-F, ^3J(F,Pt) = 468 Hz), -163.5 (*p*-F, t), -164.9 (*m*-F, br m), -165.1 (*m*-F, br m) ppm. ^{13}C{^{1}H} NMR (100.624 MHz, CD_2Cl_2, 298 K): δ = 163.5 (s, C15), 155.6 (s, C12), 152.8(s, C21), 146.8 (s, C2), 142.3 (s, C11), 140.8 (s, C17), 138.7 (s, C4), 137.2 (s, C22), 136.5 (s, C10), 134.6 (s, ^2J(C,Pt) = 110 Hz, C9), 134.4 (s, C14), 130.7 (s, C23), 130.4 (s, C6), 130.1 (s, C8), 128.4 (s, C19), 127.7 (s, C13), 124.5 (s, C16), 123.7 (s, C5), 123.2 (s, C7), 122.6 (s, C3), 120.5 (s, C18), 118.4 (s, C20) ppm. Mass spectra MALDI+ DCTB: *m/z* = 531.0 [Pt($C_{13}H_8N$)($C_{10}H_8NOH$)-H]$^+$, 699.0 [Pt($C_{13}H_8N$)(C_6F_5)($C_{10}H_8NOH$)-H]$^+$. Elemental analysis calcd (%) for $C_{29}H_{17}F_5N_2OPt$: C 49.79, H 2.45, N 4.01; found: C 49.87, H 2.14, N 4.10.

Preparation of (NBu$_4$)[Li{Pt(C_6F_5)(bzq)(8-hydroxyquinolinate)}$_2$] (3). To a solution of **1** (0.343 g, 0.500 mmol) in tetrahydrofuran (60 mL) at 195 K and under Ar atmosphere, BuLi (2.5 M solution in hexane; 0.220 ml, 0.550 mmol) was added. After 60 min of stirring the solution was allowed to reach room temperature and the solution was hydrolyzed for ten minutes to remove the excess of BuLi. The solution was evaporated to dryness and the yellow solid was treated with ^{i}PrOH (10 mL) and NBu_4ClO_4 (0.085 g, 0.250 mmol) was added. The resultant yellow suspension was filtered off, washed with *n*-hexane (10 mL) and air dried. Yield 0.281 g (0.174 mmol), 68% yield. IR υ = 2964 (vw), 1567 (vw), 1493 (m), 1450 (m), 1436 (m), 1276 (vw), 1055 (m), 951 (s), 880 (w), 796 (m, C_6F_5, X-sensitive vibr.)[47], 409 (w) cm^{-1}. ^{1}H NMR (400.132 MHz, CD_2Cl_2, 298 K): δ = 9.10 (2H, dd, ^3J(H2,H3) = 5.1 Hz, ^4J(H2,H4) = 0.9, H2, see Scheme 2 for the hydrogen and carbon numbering scheme), 8.14 (2H, dd, ^3J(H17,H16) = 8.4 Hz, ^4J(H17,H15) = 1.4 Hz, H17), 7.90 (2H, dd, ^3J(H15,H16) = 4.1 Hz, ^4J(H15,H17) = 1.4 Hz, H15), 7.74 (2H, d, ^3J(H20,H19) = 7.8 Hz, H20), 7.44 (2H, d, ^3J(H6,H5) = 8.7 Hz, H6), 7.38 (2H, d, ^3J(H7,H8) = 7.6 Hz, H7), 7.22 (2H, t, ^3J(H19,H20) = ^3J(H19,H18) = 8.0 Hz, H19), 7.20 (2H, dd, ^3J(H16,H17) = 8.4 Hz, ^3J(H16,H15) = 4.1 Hz, H16), 7.11 (2H, t, ^3J(H8,H9) = ^3J(H8,H7) = 7.5 Hz, H8), 6.97 (2H, dd, ^3J(H18,H19) = 8.0 Hz, ^4J(H18,H20) = 0.8 Hz, H18), 6.86 (4H, d, overlapped signals of H5 and H9), 6.67 (2H, d,

^{3}J(H4,H3) = 8.0 Hz, H4), 6.17 (2H, dd, ^{3}J(H3,H4) = 8.0 Hz, ^{3}J(H3,H2) = 5.1 Hz, H3), 2.70 (16H, m, α-CH_2-NBu_4^+), 1.28 (16H, m, β-CH_2-NBu_4^+), 1.13 (16H, m, γ-CH_2-NBu_4^+), 0.84 (24H, t, CH_3-NBu_4^+) ppm. ^{19}F NMR (376.479 MHz, CD_2Cl_2, 298 K): $\tilde{\delta}$ = -117.5 (2*o*-F, m, ^{3}J(F,Pt) = 597 Hz), -166.6 (*m*-F, br m), -167.0 (*m*-F, br m), -167.3 (*p*-F, t) ppm. ^{13}C {^{1}H} NMR (100.624 MHz, CD_2Cl_2, 298 K): δ = 166.2 (s, C21), 153.6 (s, C12), 148.7 (s, C2), 146.0 (s, C15), 145.2 (s, C22), 142.8 (s, C11), 137.6 (s, C10), 136.7 (s, C17), 134.0 (s, C4), 133.4 (s, C14), 133.3 (s, ^{2}J(C,Pt) = 139 Hz, C9), 130.2 (s, C23), 129.0 (s, C8), 128.6 (s, C19), 127.8 (s, C6), 125.0 (s, C13), 123.8 (s, C5), 122.3 (s, C3), 121.0 (s, C16), 119.7 (s, C7), 114.9 (s, C20), 111.4 (s, C18), 59.0 (s, α-CH_2-NBu_4^+), 24.1 (s, β-CH_2-NBu_4^+), 20.0 (s, γ-CH_2-NBu_4^+), 13.8 (s, CH_3-NBu_4^+). Mass spectra MALDI$^-$ DCTB: *m/z* = 557.0 [Pt($C_{13}H_8N$)(C_6F_5)(OH)], 684.0 [Pt($C_{13}H_8N$)(C_6F_5)(C_9H_8NOH)-H]$^+$, 1375.0 [(Pt($C_{13}H_8N$)(C_6F_5)(C_9H_6NO))Li(Pt($C_{13}H_8N$)(C_6F_5)(C_9H_6NO)]$^-$. Elemental analysis calcd (%) for $C_{72}H_{64}F_{10}LiN_5O_2Pt_2$: C 53.43, H 3.99, N 4.33; found: C 53.19, H 3.88, N 3.92.

Preparation of (NBu$_4$)[Li{Pt(C$_6$F$_5$)(bzq)(2-methyl-8-hydroxyquinolinate)}$_2$] (4). To a solution of **2** (0.350 g, 0.500 mmol) in tetrahydrofuran (60 mL) at 195 K and under Ar atmosphere, BuLi (2.5 M solution in hexane; 0.220 ml, 0.550 mmol) was added. After 60 min of stirring the solution was allowed to reach room temperature and the solution was hydrolyzed for ten minutes to remove the excess of BuLi. The solution was evaporated to dryness and the yellow solid was treated with ^{i}PrOH (10 mL) and NBu_4ClO_4 (0.085 g, 0.250 mmol) was added. The resultant yellow suspension was filtered off, washed with *n*-hexane (10 mL) and air dried. Yield 0.284 g (0.173 mmol), 69% yield. IR υ = 2963 (vw), 1562 (vw), 1496 (m), 1450 (m), 1435 (m), 1274 (vw), 1057 (m), 952 (s), 880 (w), 796 (m, C_6F_5, X-sensitive vibr.)[47], 356 (w) cm^{-1}. ^{1}H NMR (400.132 MHz, CD_2Cl_2, 298 K): δ = 9.10 (2H, d, ^{3}J(H2,H3) = 5.1 Hz, H2, see Scheme 2 for the hydrogen and carbon numbering scheme), 8.03 (2H, d, ^{3}J(H17,H16) = 8.4 Hz, H17), 7.74 (2H, d, ^{3}J(H20,H19) = 7.8 Hz, H20), 7.42 (2H, d, ^{3}J(H6,H5) = 8.7 Hz, H6), 7.38 (2H, d, ^{3}J(H7,H8) = 7.8 Hz, H7), 7.15 (2H, t, ^{3}J(H19,H20) = ^{3}J(H19,H18) = 7.8 Hz, H19), 7.11 (2H, t, ^{3}J(H8,H9) = ^{3}J(H8,H7) = 7.8 Hz, H8), 7.09 (2H, d, ^{3}J(H16,H17) = 8.4 Hz, H16), 6.90 (2H, d, ^{3}J(H18,H19) = 7.8 Hz, H18), 6.84 (2H, d, ^{3}J(H5,H6) = 8.7 Hz, H5), 6.82 (2H, d, ^{3}J(H9,H8) = 7.8 Hz, H9), 6.65 (2H, d, ^{3}J(H4,H3) = 8.0 Hz, H4), 6.21 (2H, dd, ^{3}J(H3,H4) = 8.0 Hz, ^{4}J(H3,H2) = 5.1 Hz, H3), 2.71 (16H, m, α-CH_2-NBu_4^+), 1.29 (16H, m, β-CH_2-NBu_4^+), 1.14 (16H, m, γ-CH_2-NBu_4^+), 0.85 (24H, t, CH_3-NBu_4^+) ppm. ^{19}F NMR (376.479 MHz, CD_2Cl_2, 298 K): δ = -117.2 (*o*-F, m, ^{3}J(F,Pt) = 557 Hz), -117.7 (*o*-F, m, ^{3}J(F,Pt) = 549 Hz), -166.8 (*m*-F, br m), -167.1 (*m*-F, br m), -167.6 (*p*-F, t) ppm. ^{13}C {^{1}H} NMR (100.624 MHz, CD_2Cl_2, 298 K): δ 165.6 (s, C21), 155.5 (s, C15),

153.5 (s, C12), 148.7 (s, C2), 144.3 (s, C22), 142.8 (s, C11), 138.0 (s, C10), 137.1 (s, C17), 134.0 (s, C4), 133.4 (s, C14), 133.1 (s, ^{2}J(C,Pt) = 101 Hz, C9), 129.0 (s, C8), 128.3 (s, C23), 127.7 (s, C6), 127.6 (s, C19), 125.0 (s, C13), 124.0 (s, C5), 122.4 (s, C3), 121.7 (s, C16), 119.6 (s, C7), 115.1 (s, C20), 111.4 (s, C18), 58.9 (s, α-CH_2-NBu_4^+), 24.1 (s, β-CH_2-NBu_4^+), 23.5 (s, γ-CH_2-NBu_4^+), 20.0 (s, CH_3-NBu_4^+). Mass spectra MALDI$^-$ DCTB: *m/z* = 698.0 $[Pt(C_{13}H_8N)(C_6F_5)(C_{10}H_8NOH)-H]^+$, 1403.0 $[(Pt(C_{13}H_8N)(C_6F_5)(C_{10}H_8NO))Li(Pt(C_{13}H_8N)(C_6F_5)(C_{10}H_8NO)]^-$. Elemental analysis calcd (%) for $C_{74}H_{68}F_{10}LiN_5O_2Pt_2$: C 53.98, H 4.16, N 4.25; found: C 53.66, H 4.33, N 3.99.

X-ray structure determinations. Crystal data and other details of the structure analyses are presented in Table 7. Suitable crystals for X-ray diffraction studies were obtained by slow diffusion of *n*-hexane into concentrated solutions of the complexes in 3 mL of CH_2Cl_2 (**1, 3** and **4**) or $CHCl_3$ (**2**). Crystals were mounted at the end of quartz fibres. X-ray intensity data were collected on an Oxford Diffraction Xcalibur diffractometer. The diffraction frames were integrated and corrected for absorption using the CrysAlis RED program.[48] The structures were solved by Patterson and Fourier methods and refined by full-matrix least squares on F^2 with SHELXL-97.[49] All non-hydrogen atoms were assigned anisotropic displacement parameters and refined without positional constraints, except as noted below. For **1**·CH_2Cl_2, **3**·1.875CH_2Cl_2, and **4a**·2CH_2Cl_2, all hydrogen atoms were constrained to idealized geometries and assigned isotropic displacement parameters equal to 1.2 times the U_{iso} values of their attached parent atoms (1.5 times for the methyl hydrogen atoms), with the exception of the position of the hydrogen attached to the OH group of the hydroxyquinoline ligand (H(1)) in complex **1**·CH_2Cl_2, which was found in the electron density maps and allow to refine with no positional or thermal restraints. For **2**·$CHCl_3$, the position all hydrogen atoms were found in the electron density maps and allow to refine with no positional or thermal restraints. In the structure of **3**·1.875CH_2Cl_2, the dichloromethane solvent molecules were very diffuse and restraints in their geometry and thermal parameters were used. In the structure of **4a**·2CH_2Cl_2, the γ-CH_2 and CH_3 groups of two of the butyl chains of the cation are disordered over two sets of positions refined with occupancy 0.7/0.3 and 0.6/0.4. Restraints were used in the geometry parameters involving these atoms. Full-matrix least-squares refinement of these models against F^2 converged to final residual indices given in Table 7.

CCDC-950300 (**1**), CCDC-950301 (**2**), CCDC-950302 (**3**), CCDC-950303 (**4a**) and CCDC-950304 (**4b**) contain the supplementary crystallographic data for this paper. These data can be obtained free of charge from The Cambridge Crystallographic Data Centre via www.ccdc.cam.ac.uk/data_request/cif.

Computational details. Quantum mechanical calculations were performed with the Gaussian09 package[50] at the DFT/M06 level of theory.[51] SDD basis set and its corresponding effective core potentials were used to describe the platinum atom.[52] An additional set of f-type functions was also added.[53] Carbon, fluorine, hydrogen, nitrogen and oxygen atoms were described with a 6-31G* basis set[54] except for the hydrogen atoms close to the metal (hydroxyl and methyl hydrogen atoms), which were described with a 6-31G** basis set.[55] The structures of the platinum complexes and hydroxyquinoline ligands were fully optimized with these basis sets and with no symmetry restrictions. All minima were subsequently characterized by analytically computing the Hessian matrix. Atomic coordinates (*x* ,*y*, *z*) for the optimized structures are collected in the supplementary material (Tables S3-S6). Topological analyses of the electron density distribution functions $\rho(\mathbf{r})$ were performed by using the AIMAll program package[56] based on the extended wave function obtained by M06 calculations. The AIM extended wave function format allows QTAIM analyses of molecular systems containing heavy atoms described with ECP. Atomic charges were calculated by using the natural bond orbital (NBO) analysis option as incorporated in Gaussian 09.[57] NMR chemical shifts were calculated on the previously optimized structures, but using the 6-311++g(d) basis set for all the light atoms in the molecules.[58,59]

Acknowledgments. This work was supported by the Spanish MICINN (DGPTC/FEDER) (Project CTQ2008-06669-C02-01/BQU) and MINECO (CTQ2012-35251), the Gobierno de Aragón (Grupo Consolidado E21: Química Inorgánica y de los Compuestos Organometálicos), and the Universidad de Zaragoza (JIUZ2012-CIE-02). The authors thank the Instituto de Biocomputación y Física de Sistemas Complejos (BIFI) and the Centro de Supercomputación de Galicia (CESGA) for generous allocation of computational resources.

Supporting Information. Further details of the structure determinations of **1**·CH_2Cl_2, **2**·$CHCl_3$, **3**·1.875CH_2Cl_2, **4a**·2CH_2Cl_2, and **4b**·CH_2Cl_2 in cif format. Tables of Selected bond lengths and angles, crystal data and structure refinement, and a view of the molecular structure for **4b**. Tables of atomic coordinates for the optimized structures of **1-DFT**, **2-DFT**, **A-DFT** and **B-DFT**. Table of Calculated NBO and Mulliken atomic charges for complexes **1-DFT**, **2-DFT**, **A-DFT** and **B-DFT.** Overlay drawings of the X-ray diffraction and DFT calculated structures of **1** and **2**. This material is available free of charge via the Internet at http://pubs.acs.org.

References

(1) Brookhart, M.; Green, M. L. H.; Parkin, G. *PNAS* **2007**, *104*, 6908-6914.

(2) Brammer, L. *Dalton Trans.* **2003**, 3145-3157.

(3) Martín, A. *J. Chem. Ed.* **1999**, *76*, 578-583.

(4) Brookhart, M.; Green, M. L. H. *J. Organomet. Chem.* **1983**, *250*, 395-408.

(5) Epstein, L. M.; Shubina, E. S. *Coord. Chem. Rev.* **2002**, *231*, 165-181.

(6) Casas, J. M.; Falvello, L. R.; Forniés, J.; Martín, A.; Welch, A. J. *Inorg. Chem.* **1996**, *35*, 6009-6014.

(7) Casas, J. M.; Forniés, J.; Martín, A. *J. Chem. Soc. Dalton Trans.* **1997**, 1559-1563.

(8) Falvello, L. R. *Angew. Chem. Int. Ed.* **2010**, *49*, 10045-10047.

(9) Rizzato, S.; Bergès, J.; Mason, S. A.; Albinati, A.; Kozelka, J. *Angew. Chem. Int. Ed.* **2010**, *49*, 7440-7443.

(10) Chatterjee, S.; Krause, J. A.; Oliver, A. G.; Connick, W. B. *Inorg. Chem.* **2010**, *49*, 9798-9808.

(11) Zhang, Y.; Lewis, J. C.; Bergman, R. G.; Ellman, J. A.; Oldfield, E. *Organometallics* **2006**, *25*, 3515-3519.

(12) Bortolin, M.; Bucher, U. E.; Rüegger, H.; Venanzi, I. M.; Albinati, A.; Lianza, F.; Trofimenko, S. *Organometallics* **1992**, *11*, 2514-2521.

(13) Brammer, L.; Charnock, J. M.; Goggin, P. L.; Goodfellow, R. J.; Orpen, A. G.; Koetzle, T. F. *J. Chem. Soc. Dalton Trans.* **1991**, 1789-1798.

(14) Braga, D.; Grepioni, F.; Tedesco, E.; Biradha, K.; Desiraju, G. R. *Organometallics* **1997**, *16*, 1846-1856.

(15) Wehmanooyevaar, I. C. M.; Grove, D. M.; Kooijman, H.; Vandersluis, P.; Spek, A. L.; Vankoten, G. *J. Am. Chem. Soc.* **1992**, *114*, 9916-9924.

(16) Albinati, A.; Lianza, F.; Pregosin, P. S.; Muller, B. *Inorg. Chem.* **1994**, *33*, 2522-2526.

(17) Zhao, S. B.; Wang, R. Y.; Wang, S. *Organometallics* **2009**, *28*, 2572-2582.

(18) Kozelka, J.; Bergès, J.; Attias, R.; Fraitag, J. *Angew. Chem. Int. Ed.* **2000**, *39*, 198-201.

(19) Vidossich, P.; Ortuño, M. Á.; Ujaque, G.; Lledós, A. *ChemPhysChem* **2011**, *12*, 1666-1668.

(20) Bergès, J.; Fourré, I.; Pilmé, J.; Kozelka, J. *Inorg. Chem.* **2013**, *52*, 1217-1227.

(21) Li, Y.; Zhang, G.; Chen, D. *Mol. Phys.* **2012**, *110*, 179-184.

(22) Berenguer, J. R.; Lalinde, E.; Moreno, M. T.; Sánchez, S.; Torroba, J. *Inorg. Chem.* **2012**, *51*, 11665-11679.

(23) Martín, A.; Belío, U.; Fuertes, S.; Sicilia, V. *Eur. J. Inorg. Chem.* **2013**, 2231-2247.

(24) Bakhmutov, V. I. *Practical Nuclear Magnetic Resonance Relaxation for Chemists*; John Wiley & Sons: Chichester, UK, 2004.
(25) Crabtree, R. H.; Segmuller, B. E.; Uriarte, R. J. *Inorg. Chem.* **1985**, *24*, 1949-1950.
(26) Mercury CSD 3.1.1, Cambridge Crystallographic Data Centre: Cambridge, UK, 2013.
(27) Bader, R. F. W. *Atoms in Molecules-a Quantum Theory*; Oxford University Press: Oxford, 1990.
(28) Bader, R. F. W. *J. Phys. Chem. A* **1998**, *102*, 7314-7323.
(29) Popelier, P. *Atoms in Molecules: An Introduction*; Pearson Education: Harlow, 2000.
(30) Gillespie, R. J.; Popelier, P. L. A. *Chemical Bonding and Molecular Geometry*; Oxford University Press: New York, 2001.
(31) *The Quantum Theory of Atoms in Molecules*; Wiley-VCH: Weinheim (Germany), 2007.
(32) Cremer, D.; Kraka, E. *Angew. Chem. Int. Ed.* **1984**, *23*, 627-628.
(33) Arnold, W. D.; Oldfield, E. *J. Am. Chem. Soc.* **2000**, *122*, 12835-12841.
(34) Ciclosi, M.; Lloret, J.; Estevan, F.; Sanau, M.; Perez-Prieto, J. *Dalton Trans.* **2009**, 5077-5082.
(35) Espinosa, E.; Molins, E.; Lecomte, C. *Chem. Phys. Lett.* **1998**, *285*, 170-173.
(36) Espinosa, E.; Alkorta, I.; Rozas, I.; Elguero, J.; Molins, E. *Chem. Phys. Lett.* **2001**, *336*, 457-461.
(37) Rozas, I.; Alkorta, I.; Elguero, J. *J. Am. Chem. Soc.* **2000**, *122*, 11154-11161.
(38) Iwaoka, M.; Komatsu, H.; Katsuda, T.; Tomoda, S. *J. Am. Chem. Soc.* **2004**, *126*, 5309-5317.
(39) Forniés, J.; Ibáñez, S.; Martín, A.; Gil, B.; Lalinde, E.; Moreno, M. T. *Organometallics* **2004**, *23*, 3963-3975.
(40) Braga, D.; Grepioni, F. *Chem. Soc. Rev.* **2000**, *29*, 229-238.
(41) Martín, A.; Orpen, A. G. *J. Am. Chem. Soc.* **1996**, *118*, 1464-1470.
(42) Begley, W. J.; Rajeswaran, M. *Acta Cryst. Sect. E* **2006**, *62*, 1200-1202.
(43) Rajeswaran, M.; Begley, W. J.; Olson, L. P.; Huo, S. *Polyhedron* **2007**, *26*, 3653-3660.
(44) Forniés, J.; Ibáñez, S.; Martín, A.; Sanz, M.; Berenguer, J. R.; Lalinde, E.; Torroba, J. *Organometallics* **2006**, *25*, 4331-4340.
(45) Berenguer, J. R.; Díez, A.; Fernández, J.; Forniés, J.; García, A.; Gil, B.; Lalinde, E.; Moreno, M. T. *Inorg. Chem.* **2008**, *47*, 7703-7716.
(46) Forniés, J.; Gómez, J.; Lalinde, E.; Moreno, M. T. *Inorg. Chem.* **2001**, *40*, 5415-5419.
(47) Maslowsky, E. J. *Vibrational Spectra of Organometallic Compounds*; Wiley: New York, 1977.

(48) CysAlis RED, CCD camera data reduction program, Oxford Diffraction: Oxford, UK, 2004.

(49) Sheldrick, G. M. *Acta Cryst.* **2008**, *A64*, 112-122.

(50) Frisch, M. J.; Trucks, G. W.; Schlegel, H. B.; Scuseria, G. E.; Robb, M. A.; Cheeseman, J. R.; Scalmani, G.; Barone, V.; Mennucci, B.; Petersson, G. A.; Nakatsuji, H.; Caricato, M.; Li, X.; Hratchian, H. P.; Izmaylov, A. F.; Bloino, J.; Zheng, G.; Sonnenberg, J. L.; Hada, M.; Ehara, M.; Toyota, K.; Fukuda, R.; Hasegawa, J.; Ishida, M.; Nakajima, T.; Honda, Y.; Kitao, O.; Nakai, H.; Vreven, T.; J. A. Montgomery, J.; Peralta, J. E.; Ogliaro, F.; Bearpark, M.; Heyd, J. J.; E. Brothers; Kudin, K. N.; Staroverov, V. N.; Kobayashi, R.; J. Normand; Raghavachari, K.; Rendell, A.; Burant, J. C.; Iyengar, S. S.; Tomasi, J.; Cossi, M.; Rega, N.; Millam, J. M.; Klene, M.; Knox, J. E.; J. B. Cross; Bakken, V.; Adamo, C.; Jaramillo, J.; Gomperts, R.; Stratmann, R. E.; Yazyev, O.; Austin, A. J.; Cammi, R.; Pomelli, C.; Ochterski, J. W.; Martin, R. L.; Morokuma, K.; Zakrzewski, V. G.; Voth, G. A.; Salvador, P.; Dannenberg, J. J.; Dapprich, S.; Daniels, A. D.; Farkas, O.; Foresman, J. B.; Ortiz, J. V.; Cioslowski, J.; Fox, D. J.; *Gaussian 09, Revision A.02*, Gaussian, Inc.: Wallingford CT, 2009.

(51) Zhao, Y.; Truhlar, D. G. *Theor. Chem. Acc.* **2008**, *120*, 215-241.

(52) Andrae, D.; Haussermann, U.; Dolg, M.; Stoll, H.; Preuss, H. *Theoretica Chimica Acta* **1990**, *77*, 123-141.

(53) Ehlers, A. W.; Böhme, M.; Dapprich, S.; Gobbi, A.; Höllwarth, A.; Jonas, V.; Köhler, K. F.; Stegmann, R.; Veldkamp, A.; Frenking, G. *Chem. Phys. Lett.* **1993**, *208*, 111-114.

(54) Hariharan, P. C.; Pople, J. A. *Theoretica Chimica Acta* **1973**, *28*, 213-222.

(55) Francl, M. M.; Pietro, W. J.; Hehre, W. J.; Binkley, J. S.; Gordon, M. S.; DeFrees, D. J.; Pople, J. A. *J. Chem. Phys.* **1982**, *77*, 3654-3665.

(56) Todd, A.; Keith, T. K.; AIMA11 (version 13.05.06); Gristmill Software: Overland Park KS, USA, 2013.

(57) Glendening, E. D.; Reed, A. E.; Carpenter, J. E.; Weinhold, F.; NBO Version 3.1.

(58) Feller, D. *Comp. Chem.* **1996**, *17*, 1571-1586.

(59) Schuchardt, K. L.; Didier, B. T.; Elsethagen, T.; Sun, L.; Gurumoorthi, V.; Chase, J.; Li, J.; Windus, T. L. *J. Chem. Inf. Model* **2007**, *47*, 1045-1052.

Table 1. Relevant structural and magnetic parameters illustrating the Pt···H-O contacts in complexes **1**, **2**, **A** and **B** (see experimental part for further details).

Complex	**1**	**2**	**A**[a]	**B**[a]
Pt···H (X ray), *Å*	2.09(4)	2.10(4)	-	2.19
Pt···H (DFT calculations, gas phase), *Å*	2.18	2.14	2.16	2.11
δ ^{1}H NMR (CD_2Cl_2), *ppm*	10.92	10.99	12.22	12.34
δ ^{1}H NMR (DFT calculations, gas phase), *ppm*	10.71	10.95	11.95	12.07
Δδ ^{1}H NMR (CD_2Cl_2), *ppm*	+2.64	+2.74	+3.70	+4.09
Δδ ^{1}H NMR (DFT calculations, gas phase), *ppm*	+3.02	+2.89	+4.26	+4.01
J_{Pt-H}, *Hz*	67.0	80.6	69	88
$T_{1,\,min}$ central signal, *s*[b]	1.55	1.47	-	-
$T_{1,\,min}$ satellites, *s*[b]	1.45	1.28	-	-
$\Delta T_{1,\,min}$	-0.10	-0.19	-	-

[a] Reference 6. [b] $T_{1,\,min}$ found at 193 K

Table 2. Selected bond lengths (Å) and angles (°) for $[Pt(C_6F_5)(bzq)(hqH)]\cdot CH_2Cl_2$ (**1**·CH_2Cl_2) and $[Pt(C_6F_5)(bzq)(hqH')]\cdot CHCl_3$ (**2**·$CHCl_3$).

	1·CH_2Cl_2	**2**·$CHCl_3$
Pt–C(17)	1.995(3)	1.990(2)
Pt–C(1)	2.012(3)	2.011(2)
Pt–N(1)	2.089(2)	2.083(2)
Pt–N(2)	2.144(2)	2.176(2)
Pt–H(1)	2.09(4)	2.10(4)
O–C(27)	1.355(4)	1.357(3)
O–H(1)	0.94(4)	0.91(4)
C(17)–Pt–C(1)	91.76(12)	92.57(9)
C(17)–Pt–N(1)	81.96(11)	81.80(8)
C(1)–Pt–N(1)	173.52(10)	174.24(8)
C(17)–Pt–N(2)	174.89(10)	174.90(8)
C(1)–Pt–N(2)	93.17(10)	90.03(8)
N(1)–Pt–N(2)	93.14(9)	95.67(7)
Pt–H(1)–O	162(4)	162(4)

Table 3. Comparison of selected distances (Å) and angles (°) obtained for **1** (X-ray, DFT), **2** (X-ray, DFT), $[Pt(C_6F_5)_3(hqH)]^-$ **A** (DFT) and **B** (X-ray,[6] DFT).

	Pt···H	H–O	O–C	Pt···H–O	H–O–C	Pt···H–O–C
1 (X ray)	2.09(4)	0.94(4)	1.355(4)	162(4)	110.2	-29.1
1-DFT	2.18	0.983	1.338	153.6	112.7	-45.3
2 (X ray)	2.10(4)	0.91(4)	1.357(3)	162(4)	109.8	-29.3
2-DFT	2.15	0.983	1.343	152.4	111.7	-50.1
A-DFT	2.16	0.99	1.329	157.8	113.0	-20.8
B (X ray)[6]	2.19	0.84	1.354(6)	160.7	108.4	-32.0
B-DFT	2.11	0.99	1.331	153.9	113.1	-33.7

Table 4. Topological characteristics of critical point Pt···H-O in complexes **1-DFT**, **2-DFT**, **A-DFT** and **B-DFT.**

Complex	**1-DFT**	**2-DFT**	**A-DFT**	**B-DFT**
$\rho(\mathbf{r})$ (au)	0.034	0.036	0.035	0.039
$\nabla^2\rho(\mathbf{r})$	0.070	0.076	0.070	0.079
Ellipt	0.028	0.034	0.028	0.034
Pt···H (Å)	2.18	2.15	2.16	2.11
BP length (Å)	2.21	2.18	2.20	2.14
Pt–CP (Å)	1.51	1.49	1.51	1.47
CP–H (Å)	0.70	0.69	0.69	0.67
$G(\mathbf{r})$ (au)	0.022	0.024	0.022	0.026
$V(\mathbf{r})$ (au)	-0.026	-0.029	-0.027	-0.032
$H(\mathbf{r})$ (au)	-0.004	-0.005	-0.005	-0.006
$G(\mathbf{r})/\rho(\mathbf{r})$	0.648	0.661	0.630	0.655
E(HB, Kcal mol^{-1})	-8.15	-9.11	-8.34	-9.92

BP: Bond path; CP: Critical point

Table 5. Selected bond lengths (Å) and angles (°) for $(NBu_4)[Li\{Pt(C_6F_5)(bzq)(hq)\}_2]\cdot 1.875CH_2Cl_2$ (**3**$\cdot 1.875CH_2Cl_2$).

Pt(1)–C(17)	1.978(4)	Pt(1)–C(1)	2.003(4)	Pt(1)–N(1)	2.076(3)
Pt(1)–O(1)	2.110(3)	Pt(2)–C(45)	1.981(4)	Pt(2)–C(29)	2.012(4)
Pt(2)–N(3)	2.071(3)	Pt(2)–O(2)	2.122(3)	Li–O(2)	1.886(7)
Li–O(1)	1.910(7)	Li–N(4)	2.030(7)	Li–N(2)	2.057(7)

C(17)–Pt(1)–C(1)	97.23(16)	C(17)–Pt(1)–N(1)	81.88(14)
C(1)–Pt(1)–N(1)	173.30(14)	C(17)–Pt(1)–O(1)	174.75(13)
C(1)–Pt(1)–O(1)	87.99(14)	N(1)–Pt(1)–O(1)	93.01(11)
C(45)–Pt(2)–C(29)	95.78(16)	C(45)–Pt(2)–N(3)	82.00(15)
C(29)–Pt(2)–N(3)	174.15(15)	C(45)–Pt(2)–O(2)	175.70(13)
C(29)–Pt(2)–O(2)	87.70(13)	N(3)–Pt(2)–O(2)	94.29(12)
O(2)–Li–O(1)	113.4(4)	O(2)–Li–N(4)	85.5(3)
O(1)–Li–N(4)	129.1(4)	O(2)–Li–N(2)	130.8(4)
O(1)–Li–N(2)	84.4(3)	N(4)–Li–N(2)	119.4(4)

Table 6. Selected bond lengths (Å) and angles (°) for $(NBu_4)[Li\{Pt(C_6F_5)(bzq)(hq')\}_2]\cdot 2CH_2Cl_2$ (**4a**·$2CH_2Cl_2$).

Pt(1)–C(17)	1.973(3)	Pt(1)–C(1)	2.003(3)	Pt(1)–N(1)	2.078(3)
Pt(1)–O(1)	2.111(2)	Pt(2)–C(46)	1.976(3)	Pt(2)–C(30)	2.002(4)
Pt(2)–N(3)	2.076(3)	Pt(2)–O(2)	2.100(2)	Li–O(2)	1.888(6)
Li–O(1)	1.903(6)	Li–N(2)	2.028(6)	Li–N(4)	2.058(6)

C(17)–Pt(1)–C(1)	96.04(13)	C(17)–Pt(1)–N(1)	81.98(12)
C(1)–Pt(1)–N(1)	174.03(12)	C(17)–Pt(1)–O(1)	175.51(11)
C(1)–Pt(1)–O(1)	88.09(11)	N(1)–Pt(1)–O(1)	94.09(10)
C(46)–Pt(2)–C(30)	95.92(14)	C(46)–Pt(2)–N(3)	81.75(13)
C(30)–Pt(2)–N(3)	175.35(12)	C(46)–Pt(2)–O(2)	176.02(11)
C(30)–Pt(2)–O(2)	87.66(11)	N(3)–Pt(2)–O(2)	94.55(10)
O(2)–Li–O(1)	115.0(3)	O(2)–Li–N(2)	128.2(3)
O(1)–Li–N(2)	85.1(2)	O(2)–Li–N(4)	84.8(2)
O(1)–Li–N(4)	127.2(3)	N(2)–Li-N(4)	121.7(3)

Table 7. Crystal data and structure refinement for complexes **1**·CH_2Cl_2, **2**·$CHCl_3$, **3**·1.875CH_2Cl_2, and **4a**·2CH_2Cl_2.

	1·CH_2Cl_2	**2**·$CHCl_3$	**3**·1.875CH_2Cl_2	**4a**·2CH_2Cl_2
Formula	$C_{28}H_{15}F_5N_2OPt$ ·CH_2Cl_2	$C_{29}H_{17}F_5N_2OPt$ ·$CHCl_3$	$C_{72}H_{64}F_{10}LiN_5O_2Pt_2$ ·1.875CH_2Cl_2	$C_{74}H_{68}F_{10}LiN_5O_2Pt_2$ ·2CH_2Cl_2
M_t	770.44	818.90	1777.64	1816.31
Crystal system	Monoclinic	Monoclinic	Triclinic	Triclinic
Space group	$P2_1/c$	$P2_1/n$	P-1	P-1
a/Å	10.3728(2)	10.9721(2)	14.3558(2)	13.8434(1)
b/Å	16.5660(3)	15.5286(2)	14.5503(2)	14.2761(2)
c/Å	15.0527(2)	16.6883(2)	17.2806(3)	18.7328(2)
α/º	90	90	78.609(1)	79.406(1)
β/º	96.075(2)	107.556(2)	81.501(1)	86.245(1)
γ/º	90	90	80.284(1)	81.744(1)
V/Å^3	2572.1(1)	2710.9(1)	3463.2(1)	3598.4(1)
Z	4	4	2	2
D_c/g cm^{-3}	1.990	2.006	1.705	1.676
T/K	100(1)	100(1)	100(1)	100(1)
μ/mm^{-1}	5.728	5.536	4.257	4.108
F(000)	1480	1576	1750	1792
2θ range/º	8.4-57.7	8.8-57.9	8.3-57.8	8.4-57.8
Collected reflections	28470	30600	76190	77177

Unique reflections	6142	6571	16370	17183
R_{int}	0.0249	0.0226	0.0337	0.0340
R_1, wR_2[a] ($I > 2\sigma(I)$)	0.0217, 0.0515	0.0174, 0.0424	0.0290, 0.0796	0.0276, 0.0745
R_1, wR_2[a] (all data)	0.0246, 0.0523	0.0191, 0.0432	0.0402, 0.0813	0.0396, 0.0769
GOF (F^2)[b]	1.048	1.059	1.040	1.024

[a] $R_1 = \sum(|F_o| - |F_c|) / \sum |F_o|$. $wR_2 = [\sum w (F_o^2 - F_c^2)^2 / \sum w(F_o^2)^2]^{1/2}$. [b] Goodness-of-fit = $[\sum w (F_o^2 - F_c^2)^2 / (n_{obs} - n_{param})]^{1/2}$.

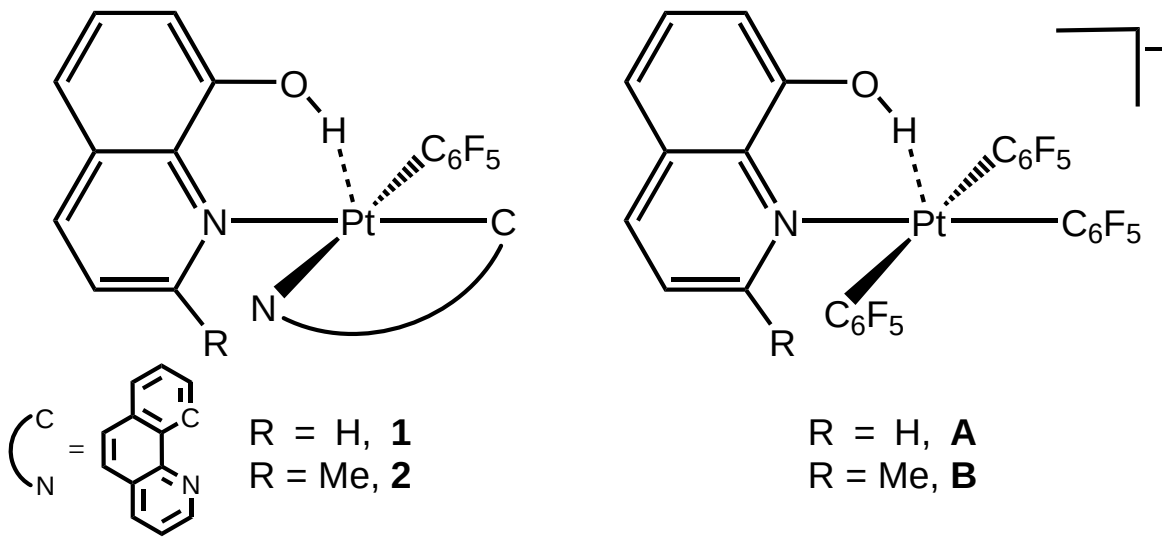

Scheme 1

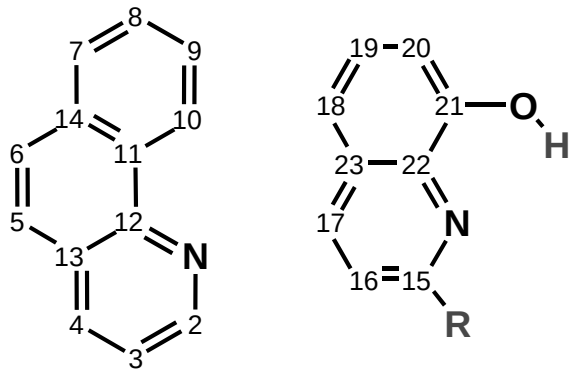

Scheme 2

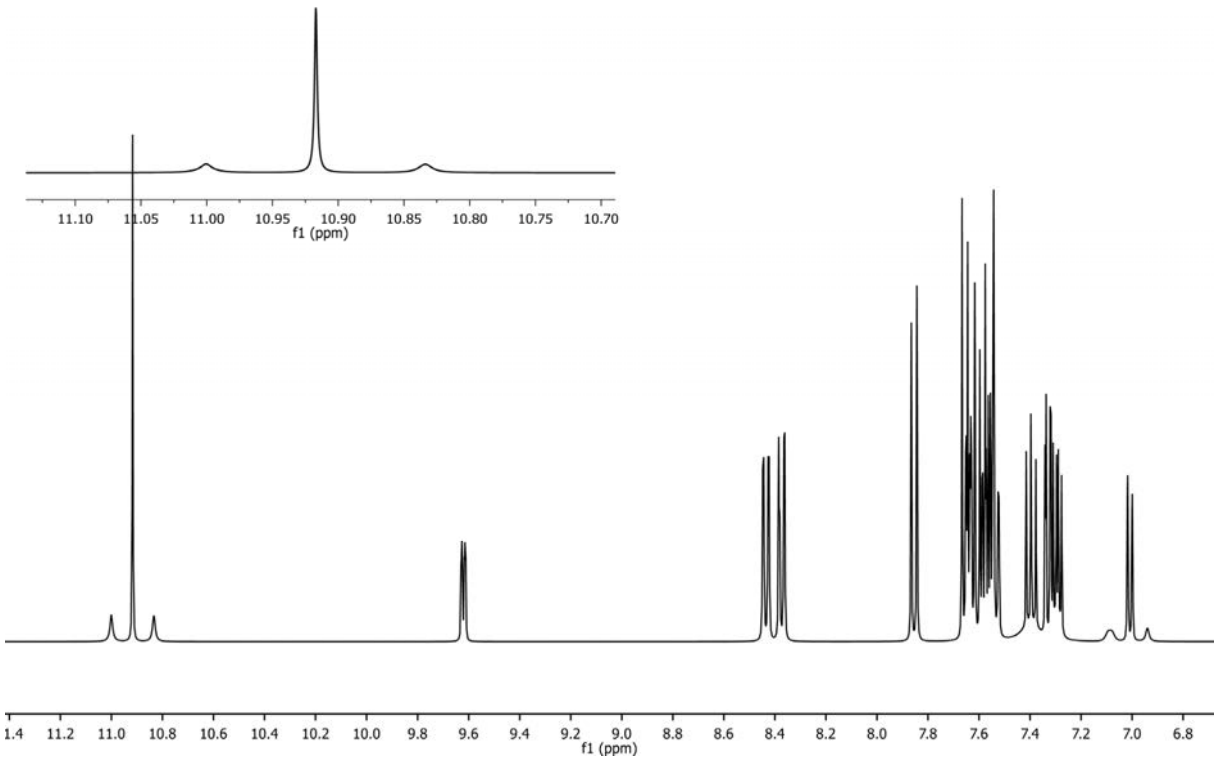

Figure 1. ^{1}H NMR spectrum of **1**. Inset: Detail of the signal of the OH hydrogen atom showing the ^{195}Pt satellites.

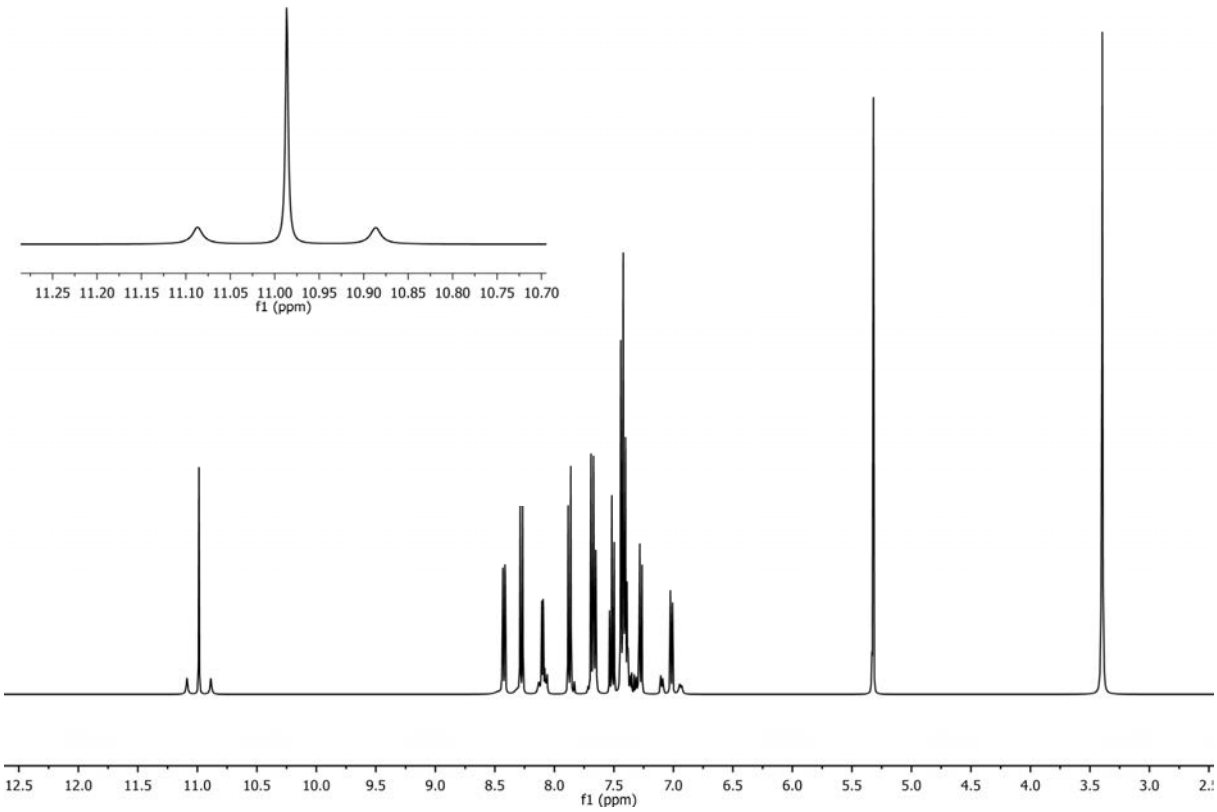

Figure 2. ^{1}H NMR spectrum of **2**. Inset: Detail of the signal of the OH hydrogen atom showing the ^{195}Pt satellites

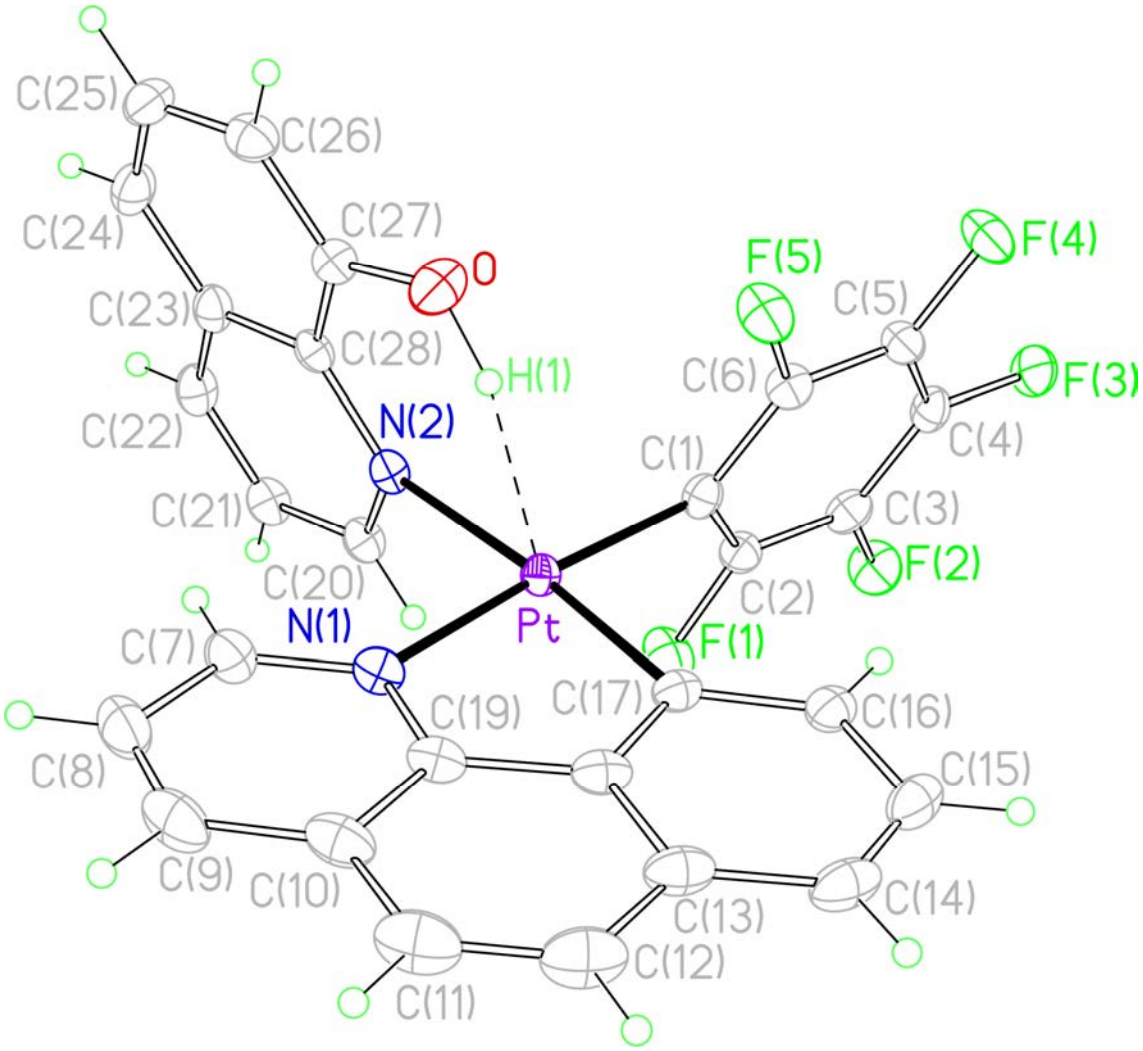

Figure 3. View of the molecular structure of the complex [Pt(C_6F_5)(bzq)(hqH)] (**1**). Ellipsoids are drawn at their 50% probability level.

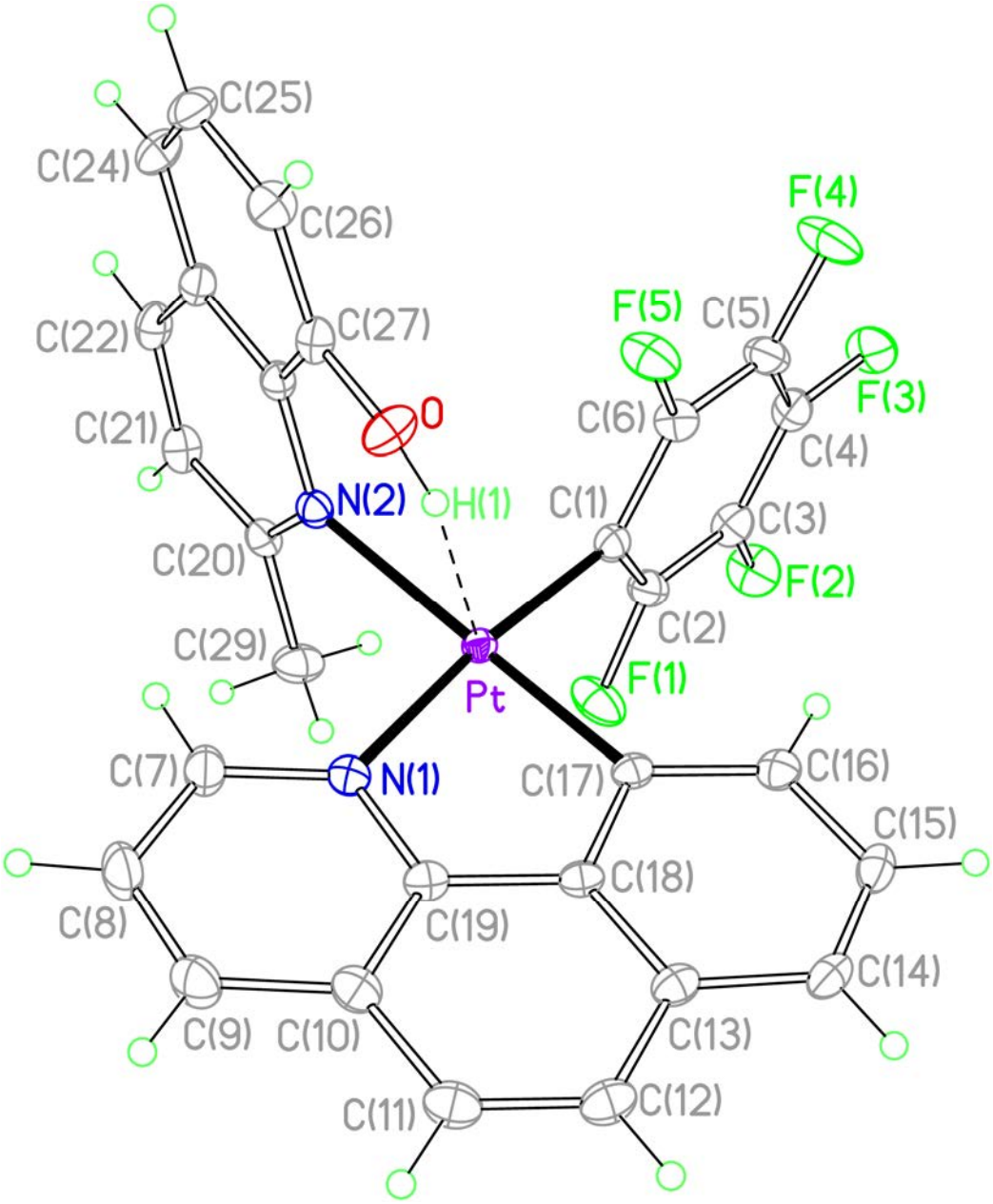

Figure 4. View of the molecular structure of the complex [Pt(C_6F_5)(bzq)(hqH')] (**2**). Ellipsoids are drawn at their 50% probability level.

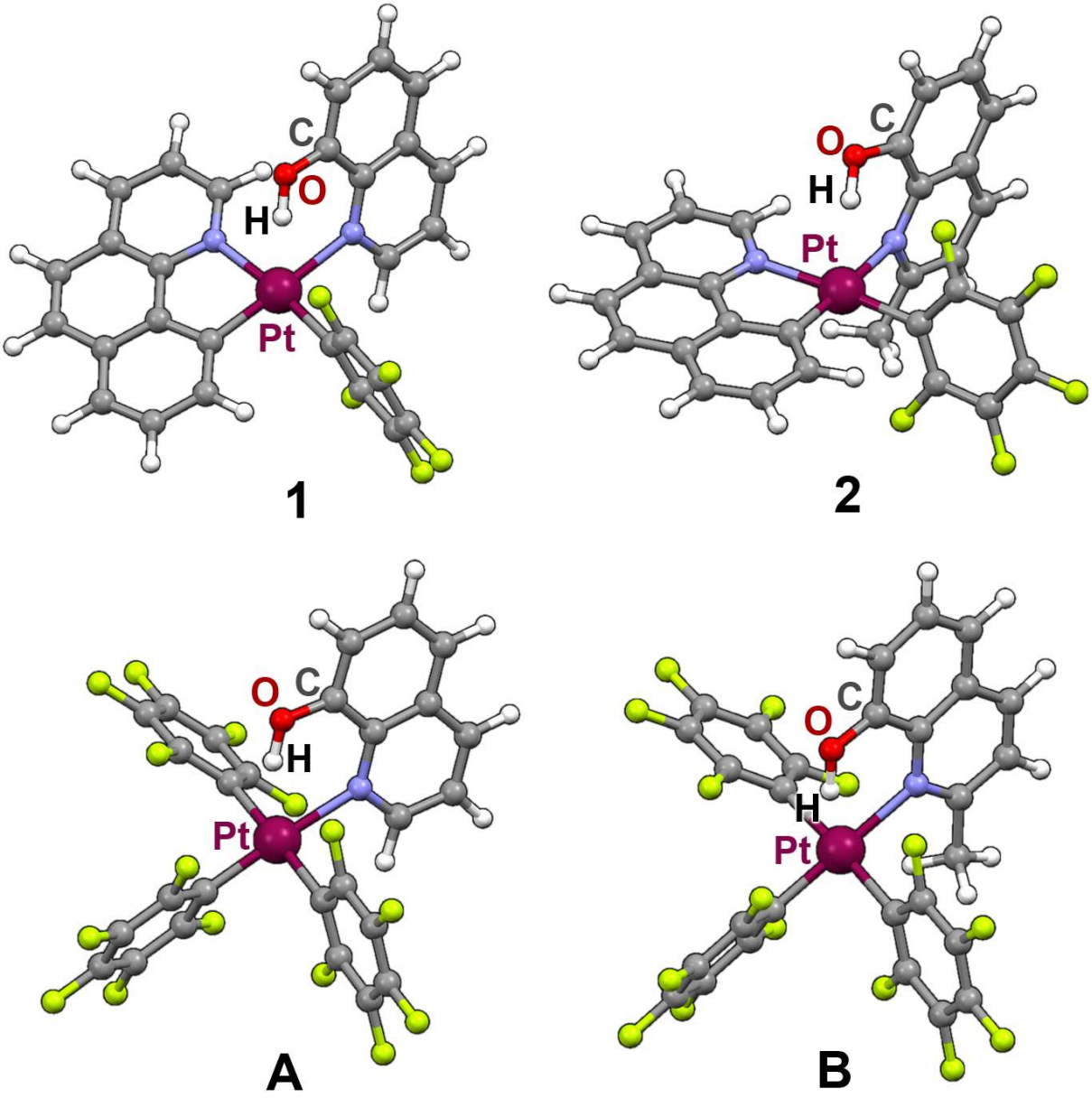

Figure 5. Optimized structures (DFT) for **1**, **2**, **A** and **B**.

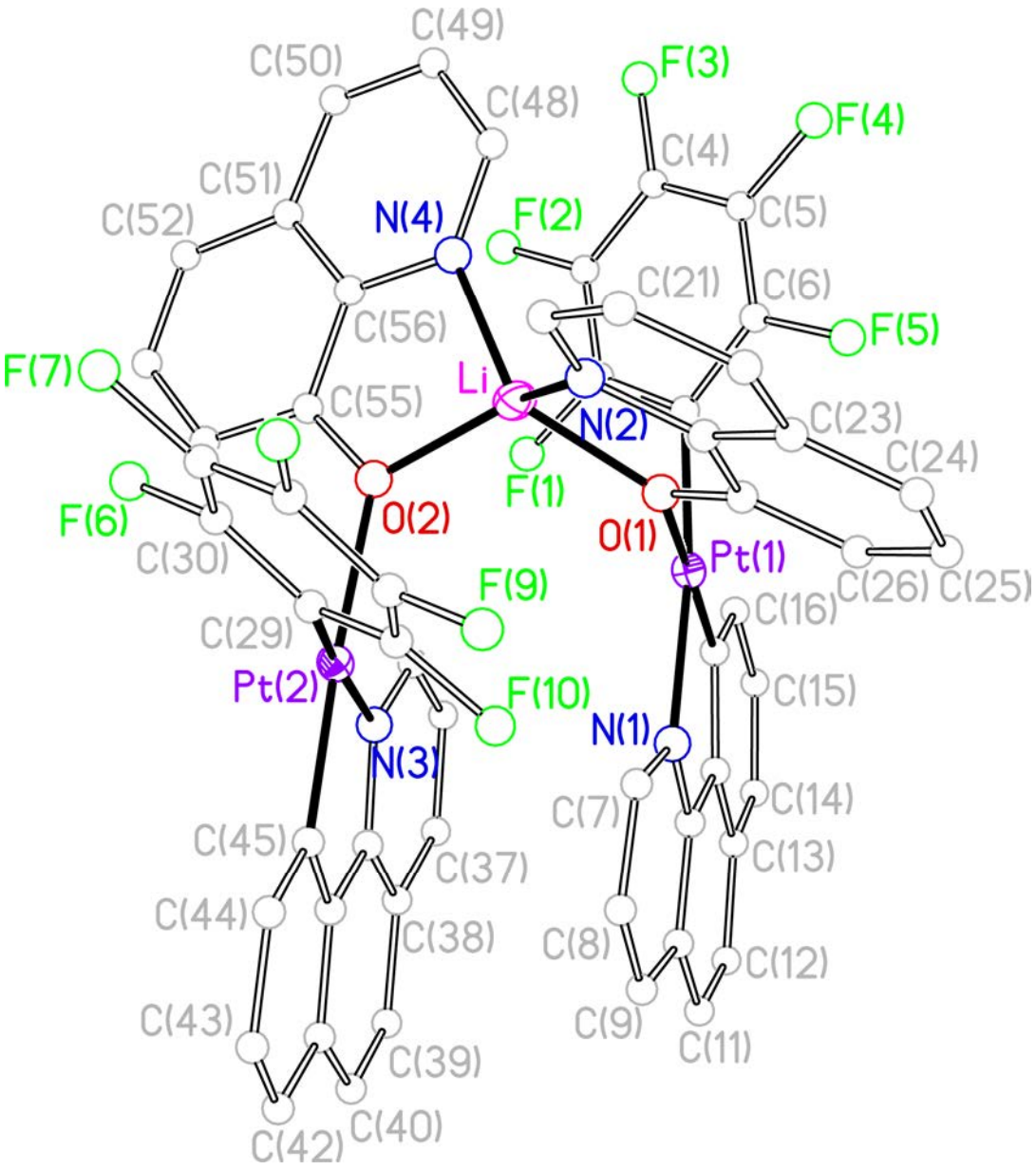

Figure 6. View of the molecular structure of the anion of the complex $(NBu_4)[Li\{Pt(C_6F_5)(bzq)(hq)\}_2]$ (**3**).

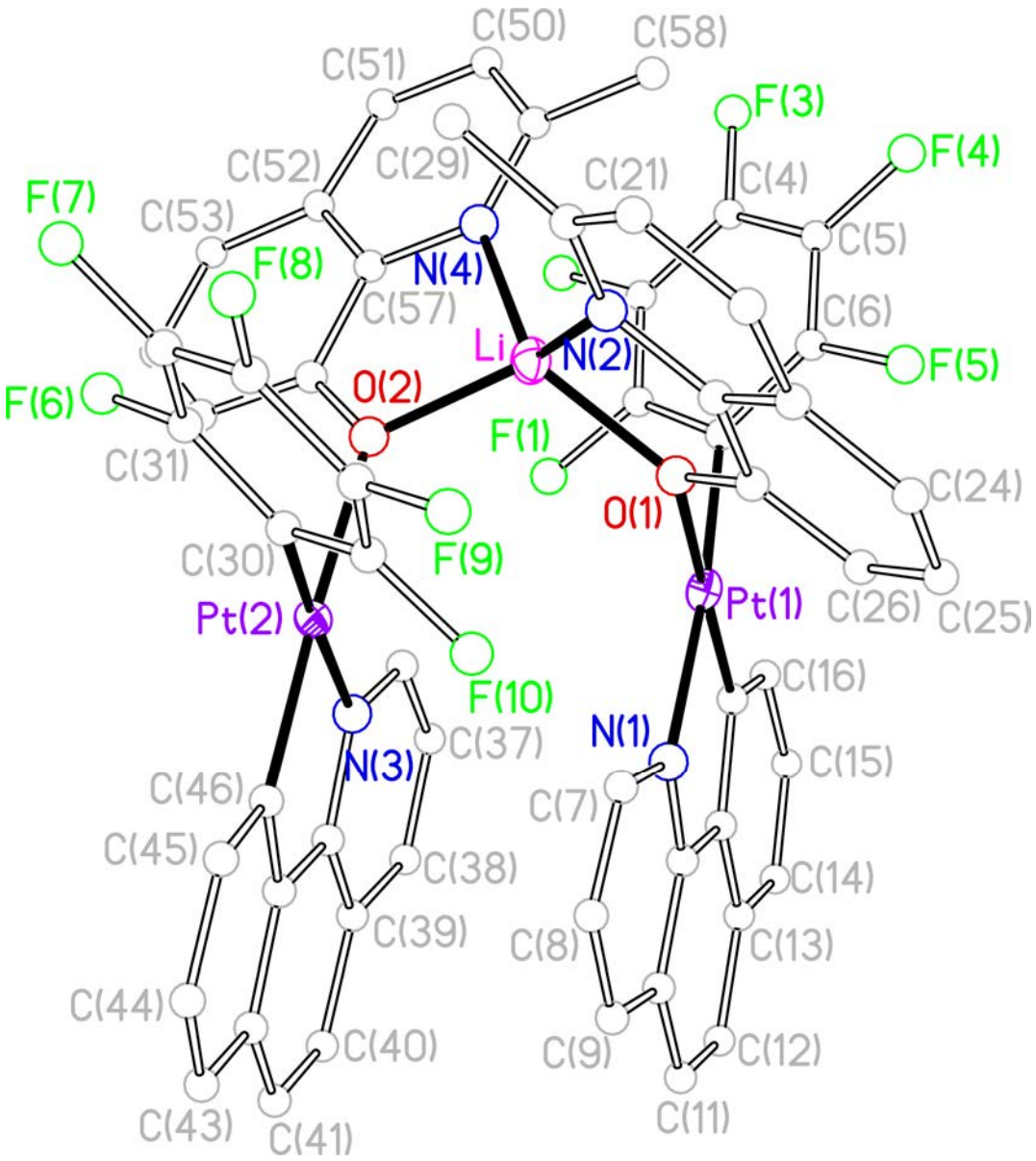

Figure 7. View of the molecular structure of the anion of the complex $(NBu_4)[Li\{Pt(C_6F_5)(bzq)(hq')\}_2]$ (triclinic pseudopolymorph, **4a**).

For use in the table of contents

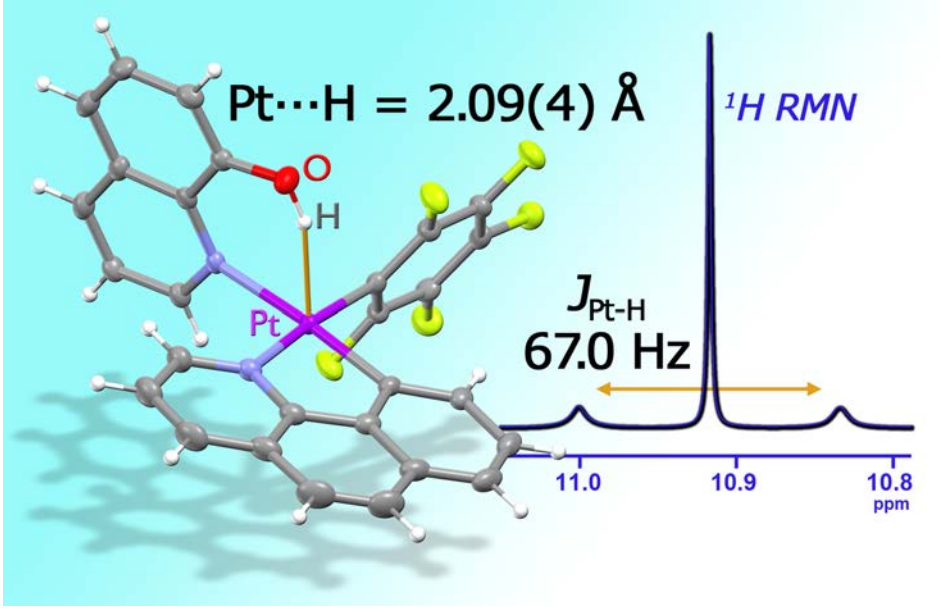

Platinum(II) complexes containing hydroxyquinoline ligands show an intramolecular hydrogen bond in which the metal center acts as the proton acceptor, both in the solid state (X-ray) and in solution (NMR). Computational studies indicate that this bond is electrostatic but with a *partial covalence*. Moreover, the amount of the downfield displacement of the ^{1}H NMR signal (typical for hydrogen bonding) is related to the difference in the charges of the H and Pt atoms.